HYBRID BASELINE LOCALIZATION FOR AUTONOMOUS UNDERWATER VEHICLES

A Thesis

Presented in Partial Fulfillment of the Requirements for the

Degree of Master of Science

with a

Major in Mechanical Engineering

in the

College of Graduate Studies

University of Idaho

by

Bryce T. Gill

December 2013

Major Professor: Eric Wolbrecht, Ph.D.

Authorization to Submit Thesis

This thesis of Bryce Gill, submitted for the degree of Master of Science with a major in Mechanical Engineering and titled "Hybrid Baseline Localization for Autonomous Underwater Vehicles," has been reviewed in final form. Permission, as indicated by the signatures and dates given below, is now granted to submit final copies to the College of Graduate Studies for approval.

Major Professor _____ Date _____
Eric Wolbrecht, Ph.D.

Committee Members _____ Date _____
Michael Anderson, Ph.D.

_____ Date _____
Dean Edwards, Ph.D.

Department Administrator _____ Date _____
John Crepeau, Ph.D.

Discipline's College Dean _____ Date _____
Larry Stauffer, Ph.D.

Final Approval and Acceptance by the College of Graduate Studies

_____ Date _____
Jie Chen, Ph.D.

Abstract

This thesis presents the hybrid baseline (HBL) navigation method for autonomous underwater vehicles (AUVs). This method seeks to improve existing navigation methods used to control a fleet of AUVs that have been developed at the University of Idaho for the purpose of measuring the magnetic disturbance caused by a surface vessel. The acquired magnetic data can be used to model the magnetic signature (i.e. disturbance field) of the vessel, enabling the deployment of magnetic field cancellation techniques to minimize susceptibility to magnetically-triggered sea mines. The accuracy of this magnetic signature model is directly dependent upon the navigational accuracy of the AUVs acquiring the data.

HBL navigation is designed as a hybrid application of independent floating transponders and moving short baseline navigation, in which acoustic ranging transponders are mounted on a moving source vessel. The AUV utilizes an extended Kalman filter (EKF) to estimate its own position, and two additional EKFs to estimate the positions of the objective ship and a nearby floating buoy. Using synchronous timing, the AUV communicates acoustically with the two surface vehicles. These communications provide the AUV with state measurements of the surface vehicles and acoustic range measurements of its own position.

The position of the buoy relative to the AUV-ship waypoint path provides the AUV with perpendicular-to-path range data (in addition to the parallel-to-path data from the ship). A MATLAB-based simulation environment was designed and used to optimize the performance of HBL navigation, and field tests were performed to verify the simulation results and evaluate the accuracy of the navigation method. After the field tests, high-accuracy position and timing data for the objective ship and floating buoy were used to recreate the path of the AUV using an optimized postprocessing EKF. The accuracy of the navigation was determined relative to AUV positions determined by an acoustic tracking array at the test facility. The resulting AUV position estimation

showed a mean error of 1.59 m, an improvement over the previous result (using moving short baseline navigation) of 3.30 m.

Acknowledgements

I would like to thank the Office of Naval Research for the financial support for this research project, as well as Doug O'Dell and the rest of the crew at the Acoustic Research Detachment in Bayview, Idaho, for all of their hard work and support throughout this testing. I would like to thank my major professor, Dr. Eric Wolbrecht, for all of his advice and assistance throughout my graduate and undergraduate careers, and my committee members Dr. Dean Edwards and Dr. Michael Anderson, for the time and help they have given me during my time at the University of Idaho. I would like to thank Dr. Michael O'Rourke for steering me towards this research project long before I had any idea what it would eventually do for me.

I would like to acknowledge all of the hard work of past researchers and students on this project, for providing much of the knowledge-base and code I have worked with in my own research. In particular I would like to thank David Schipf, Ryan Borth and John Feusi, whose aid in coding, debugging and testing was invaluable. I would especially like to thank Dr. John Canning, who has held this entire project together from beginning to end.

Finally, I would like to thank my parents for their immeasurable support over the years, and my wife Liz for helping me figure out what I want to be when I grow up.

Table of Contents

List of Figures

List of Tables

Chapter 1: Introduction

1.1: Project Background

Sea mines represent a lopsided threat to naval vessels. Their potential for damaging or destroying equipment and personnel far outweighs the costs involved in their manufacture and deployment. One of the primary methods sea mines use to trigger detonation is the detection of the magnetic field associated with a passing vessel [1]. Although mechanical countermeasures (e.g., mine sweeping) can be employed to great effect in reducing the density of a mine field, a variety of factors can lead to these methods becoming prohibitively cost- or time-intensive. To further insulate against the threat of mines, additional countermeasures are often used. In the case of magnetically-triggered mines, these typically consist of either active or passive magnetic field cancellation techniques.

Passive cancellation techniques involve onboard changes to reduce magnetic field sources. Acquiring low-field electronic equipment and replacing ferromagnetic components with non-magnetic materials are both effective passive cancellation techniques. Active cancellation consists of the installation and operation of degaussing coils. These are controllable, conducting cable coils designed to generate magnetic fields counter to those produced by the ship in which they are installed. The number and location of degaussing coils can be tailored to maximize the amount of external magnetic field reduction provided; however, each additional coil constitutes additional costs, and an additional degree of freedom that must be correctly controlled to be effective [2]. It is therefore very important to have an accurate picture of a ship's external magnetic field when utilizing this method.

Although facilities exist designed to measure a vessel's magnetic field (commonly called its magnetic signature), the applicability of the data they collect reduces as environmental conditions change. In general, a ship's magnetic field has two components: a permanent field, caused by the hull and onboard electronic and ferromagnetic devices; and an induced field, generated by motion through the Earth's background magnetic field. These can change as a ship travels to locations away from the field measurement facility. The permanent field, especially the component generated by the hull,

changes as ocean surface effects cause the vessel to flex over time during travel. The induced field depends on the strength and direction of the Earth's local magnetic field, and varies with a ship's location on the globe.

In order to address these problems, the Office of Naval Research (ONR) has tasked researchers at the University of Idaho (UI) with developing a portable method of accurately measuring the magnetic field of a naval vessel. A portable measurement method would allow a ship's degaussing system to be recalibrated as it nears a potential mine field, increasing the effectiveness of the countermeasure and the safety of the ship and crew. Due to the exponential relation between position and magnetic field strength, it is critical that the AUV position be known to a high degree of accuracy. ONR has therefore specified a maximum AUV position error of 1 meter, making the task of accurate AUV navigation a significant component of this project.

To this end, UI has developed a fleet of autonomous underwater vehicles (AUVs) equipped with magnetic field measurement and recording capabilities. The fleet's objective during the proposed magnetic signature mission will be to navigate along a pre-designated waypoint path. While the objective vessel travels counter-course to the AUVs along the same path, the AUVs will swim beneath it and collect magnetic field data.

1.2: AUV Navigation

Accurate, autonomous underwater navigation is a nontrivial endeavor. Seawater absorbs and dissipates electromagnetic wave-based signals such as radio communication; as a result, high-bandwidth continuous localization methods such as the Global Positioning System (GPS) are unavailable. Without a continuous position fix such as that from GPS, AUV navigation can be performed using only onboard sensor data – commonly called 'dead-reckoning.' This sensor data typically includes measurements from accelerometers, pressure transducers, and other tools for estimating orientation, depth and velocity. Position is then estimated using kinematic knowledge of the AUV. Because this process includes integration that is subject to drift, and the AUV experiences

disturbances such as physical waves and currents in the water, the dead-reckoned position estimate tends to diverge from the true position over time.

The traditional response to these problems is to provide the AUV with periodic absolute (or relative) position updates. Except in cases in which the AUV surfaces to re-acquire a GPS fix during the mission, this is accomplished by updating the position estimate with ranges from extra-vehicle sources using acoustic signals. Using this technique, an AUV dead-reckons during the time between range signals and updates its position when range measurements occur. In general, the use of acoustic ranging to navigate can be categorized according to the geometry of the ranging sources used.

The three primary categories of acoustic ranging geometries are Long Baseline (LBL), Short Baseline (SBL) and Ultra-Short Baseline (USBL) [3]. Alternatives to these traditional categories can also be considered, including single-source navigation methods[4], simultaneous localization and mapping (SLAM) algorithms [5], the use of communication and navigation aids (CNAs) [6], and moving baseline (MBL) approaches [7]. It is useful to understand and evaluate each of these when selecting the most appropriate navigation method to meet the requirements outlined by ONR, or when developing a new method.

LBL navigation is defined as utilizing a transponder array in which the separation distance between transponders is large relative to that between any transponder and the AUV. In general, this is accomplished by fixing the array of transponders in a perimeter around the area in which the AUV will navigate as in [8] and [9]. With depth frequently calculated using an onboard pressure transducer, horizontal planar position can be estimated using ranges from the perimeter transponders. With transponders spread around the AUV's position, this configuration is advantageous in that it helps to mitigate consistent bias in range measurements (such as that caused by an inaccurate sound speed estimate). Although previous work using the UI AUVs with an LBL positioning system has reported a navigational error of 0.74 m [10], the use of an LBL navigation system requires deployment and accurate survey an array of transponders which must remain stationary during operation (this is most readily accomplished by anchoring the transponders to the sea floor). While this method has been

demonstrated to meet the accuracy requirements specified by ONR, it does not meet the portability requirements.

SBL navigation methods have a geometric configuration opposite that of LBL: they are defined by operation in which the distance between the AUV and transponders is large relative to the distance between transponders. In practice, this has the advantage of providing a potentially more portable system than LBL navigation because there are typically fewer transponders to deploy and the spatial separation required between transponders is small compared to the desired area of operation. The experimental results shown in [11] show the advantages of this type of system: high portability when compared to LBL navigation, and high accuracy under certain conditions. A complete analysis, however, shows that this system (and other similar SBL methods) is insufficient for the goal of the current project. The accuracy achieved required the SBL array to be fixed to the sea floor with precisely known location relative to the navigation target (a dock for the AUV), and the AUV to have little or no net motion (accomplished with hovering mechanisms). SBL navigation has the important feature of being more readily convertible (compared to LBL) to a moving baseline approach due to the looser constraints on transponder number and geometry.

USBL navigation continues the trend seen to this point, further reducing the distance between transponders in the array. The transponders are often located within several centimeters of one another. As technology improves, the use of USBL methods becomes more common and more robust; recent research in Portugal [12] demonstrates successful, high-accuracy implementation of USBL techniques. Although USBL navigation can overcome the shortcomings of traditional SBL navigation, it still encounters difficulty when attempting to make the system portable. A USBL system, in general, consists of a tightly-spaced array of transponders (the baseline array) and a ranging transponder. One of these is mounted on the AUV, while the other must be fixed and have a precisely surveyed location. Usually the ranging transponder is on the AUV, with high-accuracy localization unavailable to the vehicle in real-time (data is collected and processed external to the AUV, using the USBL array). Though the work in [12] reversed this to improve onboard localization,

the requirement of a fixed ranging transponder with a known location reduces the portability of the system greatly.

Although range measurements from a single source are not sufficient to fix the AUV's position on the horizontal plane, single-source navigation methods [4] have successfully combined the ranging with onboard estimates of displacement between ranges to accurately navigate. As with USBL navigation, however, single-source navigation requires the extra-vehicle source's position to be known *a priori*, limiting portability. SLAM navigation methods operate on a similar principal: the AUV estimates its own navigation between range signals and uses the ranging data to acquire its position relative to either the local geographic features or a set of fixed transponders [5]. Although no *a priori* knowledge of the surroundings is required, a consistent geometry is necessary for successful navigation and localization. This is problematic for the proposed magnetic signature assessment mission, since the only structures near the AUV will be moving ships.

1.3: Moving Short Baseline Navigation

Recent research at UI has attempted to address the problems in current AUV navigation technology by combining the SBL concept with moving transponders. By making the baseline transponder array mobile such that it is fixed to the objective ship, a moving transponder geometry is created which allows the entire system to be portable. This moving short baseline (MSBL) navigation, though successful in addressing the portability constraint of the magnetic signature mission, falls somewhat short of the accuracy goal [7] due to the weak geometry provided by the short separation distance between transponders. The research presented herein represents an attempt to address some of the difficulties encountered in this recent work at UI.

In MSBL navigation, a pair of transponders is mounted on the objective ship to create the short baseline. As the AUV navigates, its dead-reckoned position estimate tends to degrade in accuracy as discussed previously; this is reflected in the onboard position estimate as an increase in uncertainty (the UI AUVs use an extended Kalman filter to estimate position, discussed fully in

Chapter 2). If we consider a simplified scenario in which the AUV receives ranges from both transponders simultaneously, a major source of the error found in MSBL navigation becomes clear. Fig. 1 displays two possibilities for this scenario.

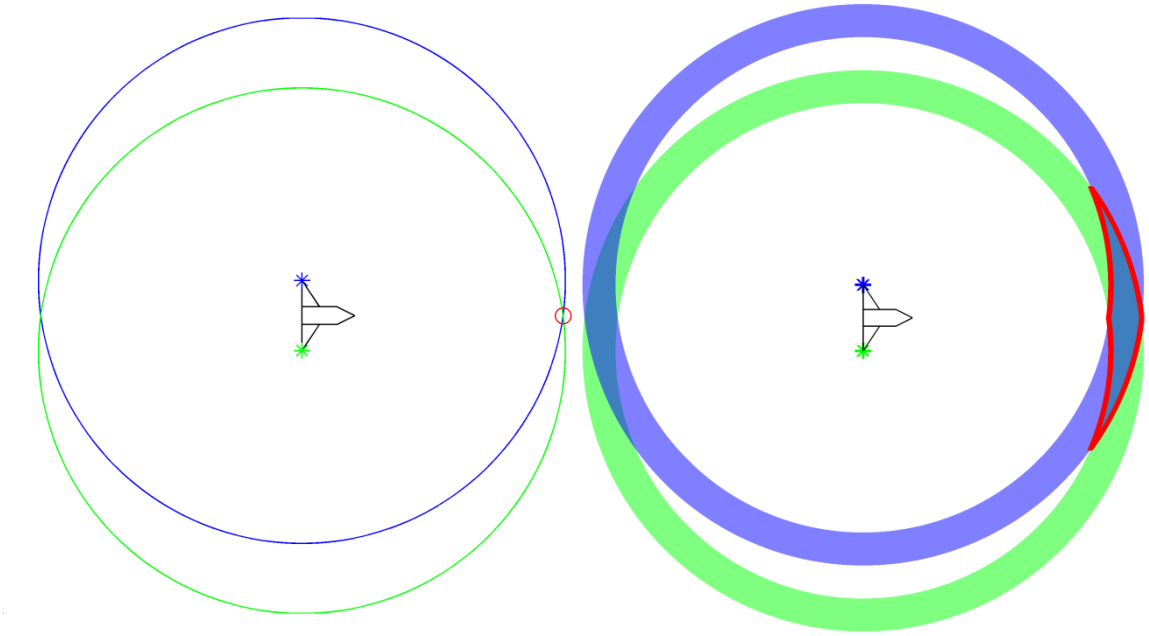

Fig. 1 A qualitative representation of MSBL ranging with exact (left) and uncertain (right) range measurements. The large circles represent ranges from the transponders located on either side of the objective ship, seen in the center of each. The red dot and red bounded area represent the exact AUV position solution and solution bound, respectively

If the ranges from the ship-mounted transponders are exact, and the transponders' positions are known exactly then the AUV position solution provided by each transponder consists of a simple circle centered on the transponder, shown in Fig. 1 (left). For any two-transponder geometry with a separation of greater than zero, this results in two circles with two intersection points: the possible locations of the AUV. Given reasonable position estimate prior to range receipt, it is possible to select one of those intersection points for an exact position. If, however, there is uncertainty in the transponders' positions or in the accuracy of the range (i.e. noise is present), then the circle solutions become band solutions as seen in Fig. 1 (right). The AUV solution is then the area in which the bands intersect; as the distance between ship and AUV is increased, the band becomes wider in the direction perpendicular to the ship-AUV path. The certainty of the position update for the AUV degrades correspondingly in that direction, reducing the quality of the position update.

What we would expect to see from MSBL navigation as a result of this analysis is a lower accuracy in position at large distances from the ship, and a higher accuracy as the AUV approaches the ship and the area encompassed by the band solution decreases. In fact, this is exactly what we see. Fig. 2 shows a typical MSBL mission with error determined relative to an independent tracking system.

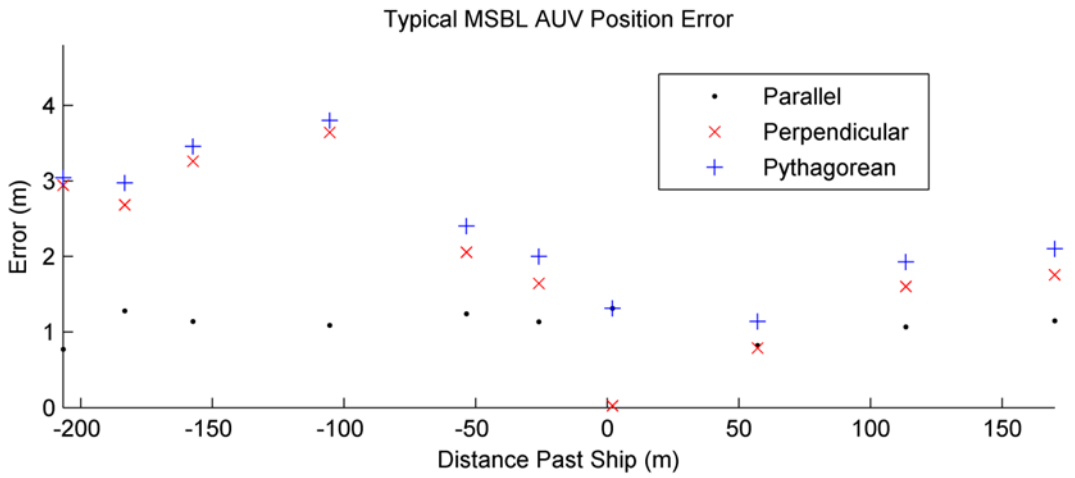

Fig. 2 AUV position error in a representative MSBL mission, compared to an independent tracking system. The AUV and ship head directly towards each other, such that the x-axis is centered on the ship's position and oriented positively in the direction behind the ship

The data in Fig. 2 is representative of MSBL missions, and is drawn from one of the missions reported in [7]. There are several important features of this data. First, it is important to note the error at the start of the mission (AUV located at ~ -200 m past the ship); due to the mission initialization and dive process, the AUV's initial position estimates can be off by as much as five meters. Next it can be seen that the parallel-to-path error is relatively constant; considering the result of the earlier qualitative analysis, this is to be expected since the parallel-to-path solution bound is relatively constant (varying primarily with changes in expected system noise and uncertainty). Finally, the perpendicular-to-path error behaves as expected as well: there is little change early in the mission, during which the qualitative solution band is wide in that direction, and accuracy improves when the AUV nears the objective ship. The net result of these three effects is an initialization error that

persists until the AUV approaches the transponder baseline. On a larger objective ship, the area in which sufficiently accurate MSBL navigation occurs is likely to be shorter than the measurement zone. As the AUV enters and traverses the measurement zone, it may still be in the process of making position corrections, causing inconsistency and inaccuracies in acquired magnetic measurements.

Further expansion on this research has altered the baseline geometry to include one or more communication and navigation aids (CNAs), additional surface vessels which can be piloted to provide the AUV with ranges from a wide variety of configurations [6]. The inclusion of CNAs represents an attempt to address the previously-discussed problems with MSBL navigation. A number of different scenarios are evaluated in which additional surface vessels, communication and navigation aids (CNAs), are equipped with transponders to modify the baseline configuration. The resulting accuracy improvements were impressive. The presence of CNAs in simulation resulted in a reported error reduction from 2.96 m to 1.55 m, an improvement of ~52% [6]. The price of this improvement, however, is high: the system cost and manpower requirements, as well as the operational complexity, are greatly increased by the inclusion of each additional surface vessel.

1.4: Hybrid Baseline Navigation

As a response to the inaccuracy present in MSBL navigation and in continuation of the work augmenting the MSBL configuration with CNAs, the research presented in this thesis proposes and evaluates a new baseline configuration with the goals of maintaining the system portability present in MSBL navigation, improving the localization accuracy earlier in the mission, and avoiding the extra costs associated with adding surface vessel CNAs. Termed hybrid baseline (HBL) navigation, this method takes advantage of the improved geometry of CNA-augmented MSBL navigation by adding a floating buoy-mounted transponder at a location off the AUV-ship waypoint path.

The geometrical advantage of this can be demonstrated with another qualitative analysis. Fig. 3 shows the effect of an adding an off-path transponder to the MSBL system. Comparing Fig. 3 to the previous presentation of MSBL navigation in Fig. 2 (right) shows the improvement. The additional

ranges, shown in black, further constrain the possible solutions for the AUV position, with the anticipated effect of a reduction in perpendicular-to-path error at large distances from the objective ship. The proposed system implementation, as shown, takes advantage of the geometrical leverage provided by a CNA craft; it does so, however, without necessitating a manned surface vehicle to provide dynamic system control. Instead, the additional transponder is to be mounted on a floating, unmanned buoy that will have either no control authority at all (drifting freely) or have a simple point-finding and station-keeping ability. Since it is at the surface, it also can be localized with GPS rather than rely on acoustic ranging for its position.

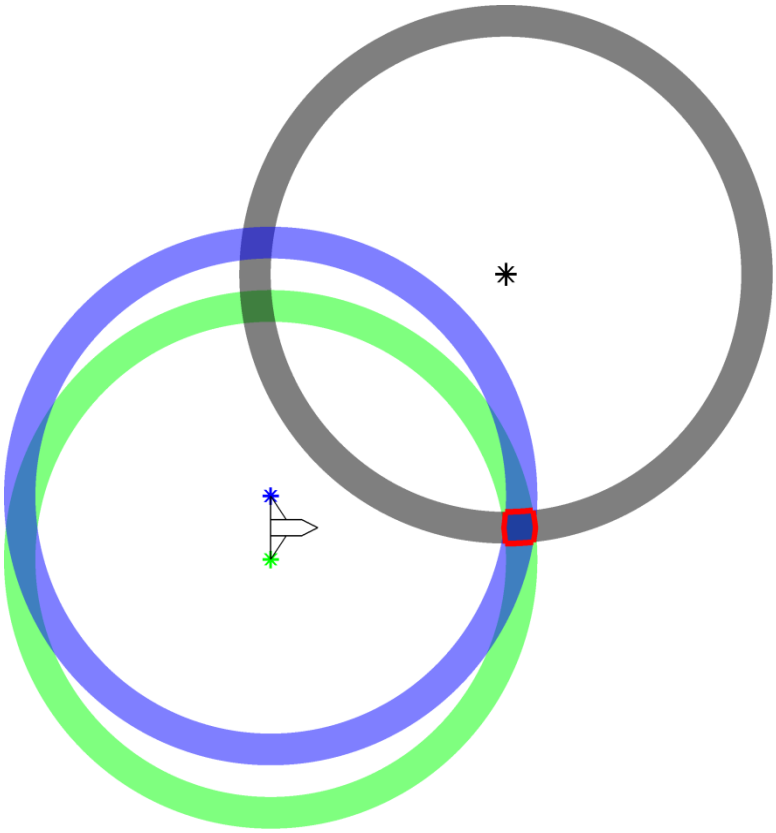

Fig. 3 A qualitative presentation of HBL navigation. Ranges from the off-path buoy provide an additional constraint on the perpendicular-to-path position estimate in MSBL navigation

In introducing HBL navigation, there are several important features to highlight before discussing the methods in-depth. The first is that there is a notable increase in system complexity with the addition of the floating buoy. Where the AUV had to track and estimate the position only of the objective ship in MSBL navigation, it now has to do the same for a separate floating vehicle. If the

buoy has no control authority and station-keeping ability, the AUV must also be capable of estimating buoy progress as it drifts.

Finally, it is worth considering the removal of a single ship-mounted transponder. Appealing again to the qualitative analysis shown in Fig. 3, it can be seen that the boundary outlined by the intersection of ranges from the buoy (black) and either ship transponder (blue or green) is not significantly different than the intersection of ranges from all three sources. It is expected, then, that in implementation this system will have similar performance with one or both ship-mounted transponders active. The research presented in this thesis will compare the navigation and localization accuracy obtained when an AUV navigates using the previously-researched MSBL method and two HBL methods: the HBL One configuration, in which only one ship-mounted transponder is active, and HBL Two configuration, in which both active. The various navigation methods considered will be evaluated and optimized in simulation, the results of which will be verified in field tests.

Chapter 2: Methods

2.1: University of Idaho AUV Design

The design of the UI fleet of AUVs is based on previous design work at the Virginia Polytechnic Institute [13]. This design was selected as a basis for the fleet based largely on its low cost and on the ease of deployment. Although not specifically required by the ONR grant funding this research, a human-deployable AUV improves testing conditions for researchers and increases the ease of operation of the final product. The current AUV design, seen in Fig. 4 has been modified from the original, including modifications to the sensor array, communication capability and computing structure.

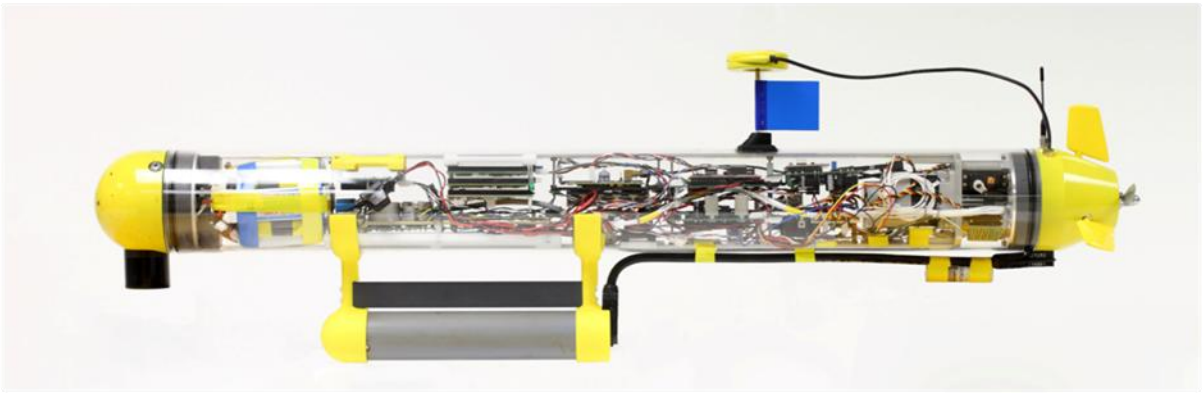

Fig. 4 A University of Idaho AUV

The AUVs have a physical profile of approximately 1 m length and 10 cm diameter, with a maximum speed of approximately 0.8 m/s in water provided by a servo motor-powered airplane propeller. Although the hull alone is calculated to withstand the pressure at a depth of approximately 260 m, the GPS receiver and various hull penetrations (e.g., the radio antenna) have not been fully evaluated for safe operation depth. The depth constraint is therefore set to 30 m for safety purposes, this value being well beyond the anticipated operational depth regime. In-mission acoustic messages are sent and received using an acoustic transducer, and pre- and post-mission communications utilize either radio packets or a locally-broadcast wireless network; further details concerning AUV communication can be found in section 2.1.2.

Each AUV has been outfitted with an array of sensors used to measure elements of its state, including: a capacitive-type pressure transducer used to calculate depth, accurate to ±0.15 m; a magnetoresistive compass used to calculate heading, accurate to ±0.5°; a two-axis micro-electro mechanical accelerometer used to calculate pitch and roll; a three-axis inertial measurement unit provides linear acceleration and angular velocities; and a GPS receiver used for localization while on the surface. In addition to these direct sensor inputs, the AUV also estimates its speed based on a known correlation between propeller RPM and vehicle velocity. Finally, the AUV also utilizes the local speed of sound in water, measured at the testing facility on the day of the test. Further details about the hardware configuration of the UI AUV can be found in [10].

2.1.1: Computation and Control

The computing core of the UI AUVs consists of distributed network of five Rabbit 3000 microcontrollers[14], programmed in the Rabbit-native language of Dynamic C. The network is designed to minimize the workload of any individual controller by assigning each a unique task. The control tasks are therefore divided into the categories of fin and motor control, data acquisition, wireless communication, acoustic communication, and mission control. The mission control board sends requests for sensor data to the data acquisition controller, sends the desired state to and requests state information from the fin and motor controller, and specifies outgoing and interprets incoming communications via the two communications controllers.

Of primary significance to the AUV research goals at UI are the path control algorithms used to maneuver the AUV along the desired course. The fin and motor controls on the AUV are manipulated to maintain depth and waypoint path independently. Using data from the accelerometer and pressure transducer, the depth controller has standard proportional and integral (PI) gains. Based on the desired depth z_d and desired pitch θ_d, the elevator position α_{EL} relative to neutral is calculated using the control law

$$\alpha_{EL} = P_z(z_d - z) + I_z \int (z_d - z) + P_\theta(\theta_d - \theta), \quad (1)$$

where z and θ are the current depth and pitch, respectively. P_z and I_z are the proportional and integral gains on the depth error, and P_θ is the proportional gain on the pitch error. Once the desired depth has been achieved, the AUV attempts to maintain a 1° downward angle of attack in order to counteract its own buoyancy.

The waypoint path controller was modeled after the Mission Oriented Operating System (MOOS) path controller designed at the Massachusetts Institute of Technology [15]. During a mission the AUV is given a series of waypoints, the path between which constitutes the desired trajectory. When the AUV is off the path an additional, virtual waypoint is used as the immediate next position goal. Shown in Fig. 5, the virtual waypoint is calculated by projecting the vehicle position onto the waypoint path and adding an optimized look-ahead distance. Use of the virtual waypoint prevents the AUV from angling directly perpendicular to the path and causing overshoot and other related undesirable behavior by providing a desired heading ψ_d for the path controller. This is used to define the heading error $E_\psi = \psi_d - \psi$. Like the depth controller, the rudder angle α_{RUD} is set with a PI controller using

$$\alpha_{RUD} = P_\psi E_\psi + P_{path} E_{path} + I_{path} \int E_{path}, \quad (2)$$

with proportional and integral gains P_{path} and I_{path} on the path error E_{path}, and proportional gain P_ψ on the heading error.

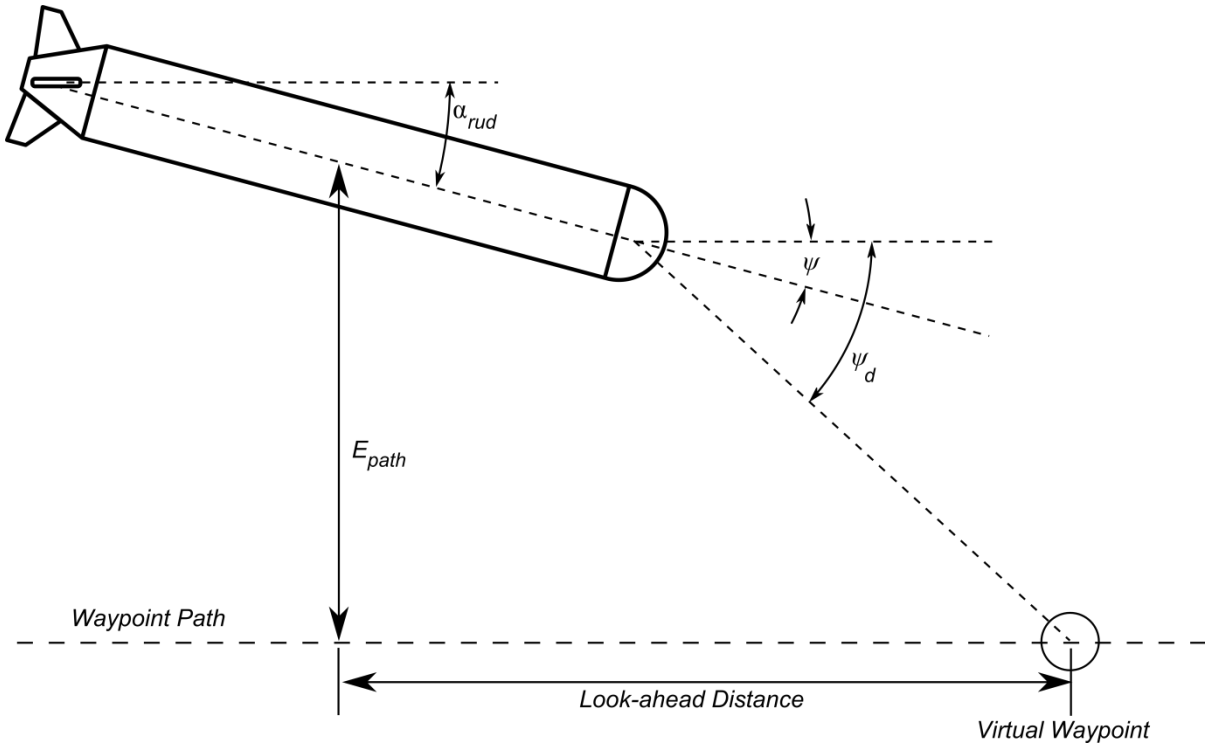

Fig. 5 An AUV navigating to the waypoint path. The MOOS-based control algorithm creates a virtual waypoint that determines the desired heading. Rudder angle is calculated using proportional gains on the heading and path errors and an integral gain on the path error

2.1.2: Communication

The UI AUVs are equipped with an acoustic micro-modem designed by the Woods Hole Oceanographic Institute (WHOI). The WHOI micro-modem, in combination with an AUV's onboard acoustic transducer, is capable of sending and receiving both 13-bit and 32-byte messages [16]. The 32-byte message takes a window of at least 6 seconds to broadcast, though commonly it is allowed 10 s to prevent message overlap and ensure successful transmission [17]. Based on previous work at UI [18], a transmission window of 2 seconds is allotted for 13-bit messages. A communication cycle based on 32-byte messages therefore has a bit rate of 20 bits/s and an acoustic range rate of 0.1 Hz, while a cycle based on 13-bit messages has a bit rate of 5.9 bits/s and a range rate of 0.5 Hz.

The analysis is further complicated when considering message success rates. Past experiments at UI [18] have shown successful transmission rates of 80% for 32-byte messages and

90% for 13-bit messages. The higher failure rate in 32-byte messages is especially significant when considered along with the high information payload: a missed message using a 32-byte communication cycle constitutes a larger loss of information than a missed 13-bit message. The same previous work at UI has concluded that a 13-bit message-based communication cycle is more effective overall for the magnetic signature mission. This type of cycle transmits sufficient data to the AUV to track a moving objective ship, while providing a greater density of ranges for absolute position measurements to the AUV.

Due to this design decision, the 13-bit message size is a limiting factor on the accuracy of measurements that must be broadcast. In order to manage the current message base and accommodate for future expansion, a five-bit header is included with each message. This reduces the effective payload to eight bits, or 2^8 distinct messages per header. All measurements to be broadcast are therefore quantized within pre-determined bounds and resolution. In field testing an area ~410 m (east) by ~150 m (north) describes the mission boundary, yielding East position quantization of 1.6 m and North position quantization of 0.6 m. Wrapping heading to 360° allows a heading quantization of 1.40625°, and a bounding vehicle speed to 4 m/s gives a speed quantization of 0.015625 m/s.

In addition to acoustic communications, the AUVs also have the capability to communicate using either radio signals or by broadcasting a short-range wireless network. Radio signals are used to initiate missions while the AUVs are on the surface. Because radio signals have a much higher bandwidth than acoustic signals, mission initialization can be done with high-accuracy information about mission parameters or the state of non-fleet vehicles (such as the objective ship). The AUV wireless network is used prior to and after missions to set onboard parameters (such as enabling synchronous WHOI modem operation or setting formation position) and to retrieve log data without removing the AUV from the watertight hull.

2.1.3: Acoustic Ranging

In acoustic range-based AUV navigation, ranges are typically acquired either asynchronously, using a two-way travel time (TWTT) method, or synchronously, using a one-way travel time (OWTT) method. TWTT ranges operate on a request-response system: the AUV sends a range request to the transponder which, after a known delay time, sends a response. The combined travel time (after removing the response delay time), along with the local speed of sound in water and the estimated vehicle motion in the interim allows the AUV to calculate its range from the transponder. This method has a significant disadvantage when operating with multiple AUVs. Since the position of each AUV is not known exactly relative to the position of the other AUVs, each must send its own ranging request. The length of the communication cycle therefore increases as the number of vehicles in the water increases. OWTT ranging, on the other hand, does not require a request from every AUV. Instead, the onboard clocks are all pre-synchronized and each transponder is assigned a time at which to broadcast; the AUVs are given this information and are then able to calculate the range based on the difference between the time of reception and the known broadcast time.

The WHOI micro-modem is able to facilitate fleet-scale operation by enabling OWTT ranging through the use of synchronous communication [19]. Using the leading edge of the pulse-per-second (PPS) signal from a GPS receiver, it is possible to accurately synch the clocks onboard the transponder and AUV. The micro-modem can be set to communicate synchronously, sending all messages at the top of the second. For distances over which the travel time is less than one second (the speed of sound in water is approximately 1500 m/s), the range *r* between AUV and transponder can easily be calculated using

$$r = tc, \tag{3}$$

where *t* is the millisecond time on the AUV onboard clock (the time since the top of the last second) and *c* is the local speed of sound in water.

It is worth noting that while submerged, the AUVs do not have access to the PPS signal from GPS. The clock drift on the UI AUV has been measured at a mean of 162 μs per hour with a standard deviation of 203 μs, resulting in a mean range error of 0.24 m after one hour [19]. Due to the comparatively short duration of submerged operation (usually less than five minutes), the drift-induced range error can be neglected for the magnetic signature mission.

2.2: State Estimation

In order to utilize both dead-reckoning tools and acoustic ranging to navigate, the UI AUVs use an extended Kalman filter (EKF). The EKF, described in general in [20] and in Appendix A, is an application of the standard linear Kalman filter to nonlinear systems. It allows the AUV to combine onboard sensor data with acoustic range data to estimate its state in real-time using a measurement model and a kinematic propagation model.

In MSBL navigation, the AUV estimates the current state of the system using two separate EKFs: one to estimate its own state, and one to estimate the state of the objective ship so that it can determine the ship-mounted transponders' locations at the time a range is received [7]. The ship EKF gives the AUV access to estimated transponder locations in the global coordinate frame; when it receives an acoustic range, this allows it to use the range to adjust its own position estimate. Insofar as the floating buoy used in HBL navigation is a moving surface vessel, it can be treated similarly to the ship. In this context, that means that an EKF can be used to estimate its position. HBL navigation therefore uses three EKFs: the AUV and objective ship EKFs used in MSBL navigation with the addition of a third for the floating buoy. For the sake of brevity, in further usage the state estimators for the AUV, ship and buoy will be referred to as the AUV, ship and buoy EKFs, respectively.

Each of the EKFs presented herein uses a kinematic propagation model $\boldsymbol{f}_{k-1}$ to predict the current state $\boldsymbol{X}_k$ in terms of the previous state $\boldsymbol{x}_{k-1}$ (with k indicating the current time step). The update model $\boldsymbol{h}_k$ describes the measurements $\boldsymbol{z}_k$ in terms of the current state. The propagation and update models are described by

$$\boldsymbol{x}_k = \boldsymbol{f}_{k-1}(\boldsymbol{x}_{k-1}, \boldsymbol{u}_{k-1}, \boldsymbol{w}_{k-1}) \quad (4)$$

and

$$\boldsymbol{z}_k = \boldsymbol{h}_k(\boldsymbol{X}_k, \boldsymbol{v}_k), \quad (5)$$

where **u** are the driving function inputs, and **w** and **v** represent the process noise and measurement noise, respectively. Throughout each of the EKFs described, the noise is assumed to be Gaussian with a zero mean.

Each EKF also has coefficient matrices **P**, **Q** and **R**, corresponding to the state estimate error covariance, the process noise covariance, and the measurement noise covariance, respectively (see Appendix A) [20]. In brief, the values in these matrices modify how the system behaves at measurement updates. For example, consider a system that at some time for a particular state has a high state estimate error covariance; if it receives a measurement of that state with a low measurement noise, it will tend to correct more towards the measured value than the current state value. The values used in these matrices are determined in part by the expected noise in the various elements of the system, and in part through an optimization process. The process by which the values are obtained will be discussed in section 2.3.3, and the values used will be given in section 3.1.3.

2.2.1: AUV State Estimation

Because the AUV can use its onboard pressure transducer to estimate depth with a high degree of accuracy at each time step, it is unnecessary to include a depth term in the state vector for EKF calculations. Instead, the depth can be treated as a constant when it appears in the EKF. We can therefore constrain the AUV's state estimation to the horizontal plane. To simplify operation the AUVs navigate using local East and North coordinates (in meters), deriving these values from the latitude and longitude data provided at various points by GPS. In order to fully define the state of the AUV such that a propagation model can be developed, the AUV's speed and heading must also be included. Past work at UI [21] has found that the magnetoresistive compass is sensitive to the same type of magnetic field disturbances being measured in a magnetic signature mission. In order to

address this, a fifth state has been added to the AUV EKF to account for compass bias resulting from improper calibration or magnetic field disturbances. The AUV state vector can therefore be described by

$$\boldsymbol{X}^A = [E^A \quad N^A \quad S^A \quad \psi^A \quad b^A]^T, \tag{6}$$

where E and N are the local east and north position, S is the speed, ψ is the heading, and b is the bias. The superscript A specifies that the term is an element in the AUV EKF. The process noise vector $\boldsymbol{w}$ has entries corresponding to each element of the state vector.

The propagation model for the AUV position assumes constant speed and heading between time steps, leveraging the fact that the parameters of the magnetic signature mission typically call for constant speed and heading. Because the vehicle speed depends on controller output to the motor, it does not follow a kinematic propagation model; it is therefore assumed constant in the kinematic propagation model and high-rate sensor data from the motor controller is used to update the value at nearly every time step using the state update model. The only driving function input to the propagation model is the rate of change in heading, drawn from the IMU. The IMU measures three orthogonal accelerations with respect the AUV frame which are transformed into the heading rate of change in the local coordinate system using an Euler angle approach [21]. Finally, the bias is assumed to be constant between states and is updated at a high rate using the measurement model, similar to the speed. The AUV propagation model takes the form of (4) with

$$\boldsymbol{f}_{k-1}^A = \begin{bmatrix} E_{k-1}^A + \Delta t\, S_{k-1}^A \sin\psi_{k-1}^A + w_E^A \\ N_{k-1}^A + \Delta t\, S_{k-1}^A \cos\psi_{k-1}^A + w_N^A \\ S_{k-1}^A + w_S^A \\ \psi_{k-1}^A + \Delta t\, \dot{\psi}_m^A + w_\psi^A \\ b_{k-1}^A + w_b^A \end{bmatrix}_{k-1}, \tag{7}$$

where Δt is the time interval between state estimates and $\dot{\psi}_m$ is the IMU-transformed z-axis acceleration.

At varying intervals during operation, measurements of different state values are taken. As previously discussed, the AUV has a number of onboard sensors; of specific import to the EKF are measurements of the speed (estimated based on motor controller output) and the heading (from the

compass). In addition to onboard sensor data, acoustic ranges also constitute measurements of the AUV's position. Because there are three possible transponders from which range measurements can be taken, the AUV EKF measurement vector is given by

$$\boldsymbol{z}^A = [r_1 \quad r_2 \quad r_3 \quad S_m^A \quad \psi_m^A]^T, \tag{8}$$

where r_{1-3} are the ranges from each transponder, S_m is the measured speed and ψ_m is the measured heading. Convention throughout this thesis will use 1 and 2 for the port and starboard ship-mounted transponders, respectively, and 3 for the buoy transponder.

The AUV measurement model relates the measurements to the states according to (5) with

$$\boldsymbol{h}_k^A = \begin{bmatrix} \sqrt{(E_k^A - E^{T_1})^2 + (N_k^A - N^{T_1})^2} + t_1 v_{tof} + c v_c \\ \sqrt{(E_k^A - E^{T_2})^2 + (N_k^A - N^{T_2})^2} + t_2 v_{tof} + c v_c \\ \sqrt{(E_k^A - E^{T_3})^2 + (N_k^A - N^{T_3})^2} + t_3 v_{tof} + c v_c \\ S_k^A + v_S^A \\ \psi_k^A + b_k^A + v_\psi^A \end{bmatrix}. \tag{9}$$

The T_{1-3} superscripts on *E* and *N* terms refer to the positions of the ranging transponders. These are drawn from the ship and buoy EKFs, and are treated as constants within the AUV EKF. The trailing two terms for each of the range measurement models represent noise dependent upon the travel time of the signal and noise in the speed of sound, where *t* is the signal travel time, *c* is the local speed of sound in water, and v_{tof} and v_c are the corresponding noise in those two measurements. The range-dependent noise term used here models the increase in uncertainty as distance to the transponder increases. Finally, the terms v_s and v_ψ are the noise terms in the speed and heading, respectively.

2.2.2: Objective Ship and Floating Buoy State Estimation

Because the ship and buoy can broadcast information about their current states directly, the EKFs required to estimate their state between broadcasts are comparatively simple. Furthermore, since the ship and buoy are both surface vessels moving in a plane, the formulation of both EKFs is identical. As such, their presentation can be condensed to that of a single EKF; for convenience here

the superscript *V* will be used for the general-purpose surface vehicle EKF and superscripts of *S* or *B* will indicate ship or buoy EKF, respectively.

For a magnetic signature mission, the objective ship will ideally be following a steady path. Even with some variation from the path (due to wind, currents, or pilot error) it can reasonably be modeled as constant-trajectory over short durations. The same assumption holds true for the buoy, which is subject to drift conditions. The propagation model for the surface vehicle EKFs, then, requires the same state information as the AUV: local east and north position, speed and heading. Because heading information in this case is acquired using a differential GPS (DGPS) system, it is unnecessary to include a compass bias term to account for magnetic disturbances. The state vector for each surface vehicle is therefore given by

$$\boldsymbol{X}^V = [E^V \quad N^V \quad S^V \quad \psi^V]^T, \tag{10}$$

with terms as previously defined. The propagation model is assumes with constant speed and heading between updates. The resulting $\boldsymbol{f}_{k-1}$ in (4) is

$$\boldsymbol{f}_{k-1}^V = \begin{bmatrix} E^V + \Delta t\, S^V \sin\psi^V + w_{E^V} \\ N^V + \Delta t\, S^V \cos\psi^V + w_{N^V} \\ S^V + w_{S^V} \\ \psi^V + w_{\psi^V} \end{bmatrix}_{k-1}. \tag{11}$$

The ship and buoy vehicle measurement models are simpler than the AUV measurement model due to the fact that the ship and buoy have direct access to their own state, and are able to broadcast that information to the AUV. The measurement vector therefore consists of the state information that can be broadcast, and the measurement update model is simply the state vector with associated noise terms. The resulting measurement model takes the form of (5), where

$$\boldsymbol{z}^V = [E_m^V \quad N_m^V \quad S_m^V \quad \psi_m^V]^T \tag{12}$$

and

$$\boldsymbol{h}_k^V = \boldsymbol{X}_k^V + \boldsymbol{w}^V, \tag{13}$$

with terms as previously defined and the subscript *m* indicating a measured value.

2.3: Optimization

Viewing HBL navigation as an extension of MSBL navigation highlights several key components of the new system that can alter its performance. The initial location of the buoy relative to the AUV-ship waypoint path can affect the geometric leverage provided by ranges from the buoy; the communication cycle can affect the frequency, quality, and reliability of updates to vehicle EKFs; and the EKF coefficient matrices can affect the behavior of the EKF at updates, or be used to bias the state estimate towards either onboard sensors or acoustic range data. Because the general system function and layout remains the same, these three components are the primary methods by which improvements to HBL navigation can be made. Therefore it is important to consider the range of possibilities for each and optimize the system accordingly.

2.3.1: Buoy Location Optimization

The first parameter of HBL navigation to be optimized is the floating buoy's initial position relative to the waypoint path. A change of the relative geometry between the AUV, ship and buoy is expected to change the effectiveness of HBL navigation, varying between optimal improvement and MSBL-level accuracy. This is qualitatively presented in Fig. 3. As the location of the buoy changes, it is possible to stretch or narrow the solution region. At buoy locations along the waypoint path, the effect of the buoy ranges will be minimal since their overlap with the ranges from the ship-mounted transponders will be large. When the line connecting the buoy and AUV is perpendicular to the waypoint path, the buoy's effect will be the greatest because the buoy range circles and ship range circles intersect at approximately right angles, minimizing the overlap space and decreasing the size of the solution bound.

In HBL navigation, the AUV and ship are both mobile; with a drifting buoy, the buoy-AUV-ship angle described above will change throughout the mission. This is further complicated because the buoy is subject to drift, which can vary widely in its velocity and direction. Due to the unpredictable variation in buoy drift speed and heading, the optimization of buoy position was

performed with a zero drift condition. Drift velocity is expected to be zero mean with a Gaussian distribution, so this zero-drift approximation is expected to improve the consistency of the optimization results. The task of this optimization therefore becomes a matter of determining the best buoy starting position in terms of its overall effectiveness for the mission.

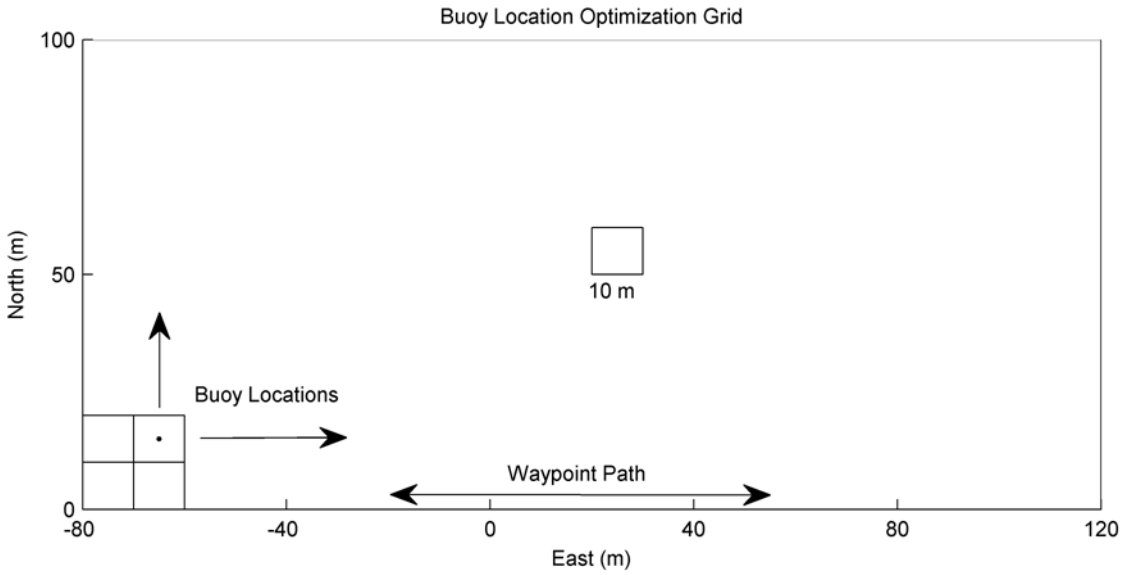

Fig. 6 Buoy location grid used during optimization. The AUV-ship waypoint path lies along the x-axis, with the AUV traveling eastward and the two vehicles crossing at approximately the origin

This optimization was performed using results from simulation. The buoy location was designated at the start of each run by iterating through locations shown in the grid described in Fig. 6. The AUV-ship waypoint path was 200 m long with a West-East orientation (AUV traveling east), providing the eastern, western and southern boundaries for the buoy location. The northern location was bounded at 100 m from the waypoint path, corresponding to two-thirds of the maximum extension of an 8-bit North position quantization at a resolution of 0.59 m. Each buoy location was evaluated using a Monte Carlo method; the metric of evaluation was the mean estimated AUV position error in the measurement zone over 250 runs at each buoy location. For this and all other evaluations given, the measurement zone is specified by the scaling method used in [7]. It describes the area between 30 m ahead of the objective ship and 75 m behind it.

2.3.2: Communication Cycle Optimization

As discussed in section 2.1.2, the WHOI micro-modem enables broadcast and receipt of both 13-bit and 32-byte acoustic messages. The advantages and disadvantages of each have been considered thoroughly for past work at UI [7]. The result has been a determination that greater frequency in range updates (using 13-bit messages) is more significant to AUV navigation accuracy than greater payload and payload accuracy per message (using 32-byte messages). HBL navigation will therefore use the modem's 13-bit message capability, with a communication cycle consisting of a series of 13-bit messages. This limits communications to a single measurement per message: a 5-bit header to specify the type of measurement, and an 8-bit payload for the measurement (see Appendix B).

The question, then, is of the sequence and content of those messages. Between the objective ship and the floating buoy, there are a total of eight possible broadcasts that the AUV can use to update the surface vehicle EKFs – one for each state of each vehicle. Because the buoy's physical design is intended to be relatively small, approximating a floating bob on the water surface, practical considerations can eliminate two of those: the rocking motion induced by waves and wind is likely to impair measurements of speed; and without a control authority the buoy is likely to turn randomly, making heading measurements ineffective.

This gives a minimum cycle length of six total broadcasts – one for each of the objective ship's states, and one each for the floating buoy's north and east states. In addition to these, a two-second window is allotted for the AUV fleet leader to broadcast its progress, enabling cooperative formation swimming, and a two-second window at the end of each cycle to allow noise to clear from the water (this helps prevent message buffering errors in the WHOI micro-modem). The structure of the cycle can be determined by considering the likely effects of different configurations. For example, a message cycle consisting of four ship broadcasts then two buoy broadcasts (in addition to the additional four seconds mentioned above) would likely minimize the effectiveness of ranges from the buoy, since both buoy ranges in the cycle would happen consecutively and the remainder of the cycle

would see the AUV functioning with no range updates from the extra transponder. It is therefore likely to be better to spread them out relatively evenly across the entire duration of the cycle. This cycle, the HBL Short cycle, can be seen in Table 1.

TABLE 1. HYBRID BASELINE COMMUNICATION CYCLES

Cycle Time (s)	**Cycle Name**	
	HBL Short	**HBL Long**
0	Ship East	Ship East
2	Ship North	Ship North
4	Buoy East	Buoy North
6	Ship Speed	Ship Speed
8	Ship Heading	Ship Heading
10	Buoy North	Buoy East
12	Fleet Leader	Fleet Leader
14	Silent	Ship East
16	---	Buoy North
18	---	Silent

Previous experience in AUV field testing has led to consideration of a second communication cycle as well. The cycle described above ("HBL Short") has a total length of 16 seconds: eight for the ship, four for the buoy, and four for the AUV leader and dead space at the end of each cycle. In past field tests it has proven useful to have a cycle that is evenly divisible into one-minute intervals, making it possible for a researcher to quickly evaluate communication timing issues. The second communication cycle considered in this optimization ("HBL Long") therefore has an additional two broadcasts added, for a total cycle length of 20 seconds. Following the same configuration analysis as above, and basing off the HBL Short cycle, the HBL Long cycle will have one additional broadcast from each surface vehicle. Based on observations from the qualitative ranging analysis from Chapter 1, it is likely that the ship's east position will be the most helpful in an extra broadcast, and the buoy's north position will be its most helpful state to broadcast in this situation. Additional broadcasts in these two communication slots will also be considered.

The optimization for this aspect of the HBL navigation system will consist of a Monte-Carlo evaluation of each possible communication cycle. In the case of a statistically insignificant or nearly insignificant difference, the HBL Long cycle will be selected due to its practical helpfulness in field testing.

2.3.3: EKF Coefficient Matrix Optimization

The EKF covariance matrices **P**, **Q**, and **R** are the second set of optimization parameters for HBL navigation. In general, these values are often considered the method of "tuning" an EKF, even though they ostensibly have values that correspond to the system the EKF is estimating. The measurement noise covariance **R**, for example, should correspond to the covariance of the expected Gaussian noise in the measurements used in an EKF. Modifying it affects the impact of measurements when the EKF updates; a lower value causes the EKF to tend to "trust" the corresponding measurement to a greater degree, forcing the state estimate to agree closer with the most recent measurements.

In HBL navigation, there are sets of coefficient matrices for three different EKFs that must be optimized. The coefficient matrices are initially all diagonal, with a diagonal length matching the corresponding state or noise vector – e.g., $\boldsymbol{P}^{A}$ is the AUV state estimate error covariance so it has a diagonal length of five, matching the length of the AUV state vector $\boldsymbol{X}^{A}$. In total, then, there are 38 values here to optimize: the AUV EKF contains five states with five corresponding process noise terms and its update model contains four measurement noise terms; and the ship and buoy EKF each consist of four states, with four corresponding process noise terms and four measurement noise terms.

This load can be reduced somewhat by relying on past work. Because the function of the ship EKF is identical to its function in MSBL navigation [7], it is not expected that further optimization in this area will yield improvement. In addition, several of the covariance terms in the AUV EKF are not expected to change from MSBL to HBL: the initial state estimate error covariance values should all remain the same because no changes have been made to mission initialization procedure; the speed,

heading and compass bias process noise terms are expected to remain the same because the AUV onboard equipment has not changed from previous operation; and the entire measurement noise covariance matrix should remain unchanged, since the measurement methods for speed, heading, speed of sound and time of flight have not been altered. Finally, none of the measurement noise covariances in the buoy EKF require optimization. Those corresponding to east and north position measurements should match those used in the ship EKF as both vehicles use the same hardware setup (differential GPS) to measure their position, and because the speed and heading are never measured, the corresponding measurement noise will have no effect on the system performance. In total, this constitutes a reduction to 10 values to optimize, down from 38. There remain ten values in the buoy EKF, as well as the process noise covariances for the AUV east and north positions.

Optimizing the buoy EKF provided a unique challenge. Using a 13-bit communication cycle, the AUV receives position updates from the surface vehicles at a maximum rate of 0.5 Hz; in the case of the buoy, using the HBL Long cycle, the AUV receives three updates in 20 s, for a net rate of 0.15 Hz. Breaking this down further, the AUV receives buoy North position updates twice per cycle (0.1 Hz), and East updates only once (0.05 Hz). Furthermore, all of these measurements have a very low resolution – 1.6 m for East, and 0.6 m for North. When drift speeds are on the order of ~0-20 cm/s, and no speed or heading measurements are given to the EKF, the kinematic propagation model behaves somewhat poorly.

Consider the example shown in Fig. 7; on the left are shown the true and broadcast positions, and on the right is one possible resulting position estimate. As in the current system design, the position measurements of the buoy are quantized (the green lines denote quantization resolution) and only one of either the East or North state measurements is broadcast at a given time. In Fig. 7 (right), the EKF behavior shown is the result of allowing the measurement model to determine the speed and heading states. In this example, the buoy EKF has a low covariance for its position measurements and a moderate process noise covariance in its speed and heading states. The resulting is that the speed

and heading states of the EKF adjust to compensate for the large jumps in position measurement (due to measurement quantization), and the predictive behavior for the buoy position is somewhat erratic.

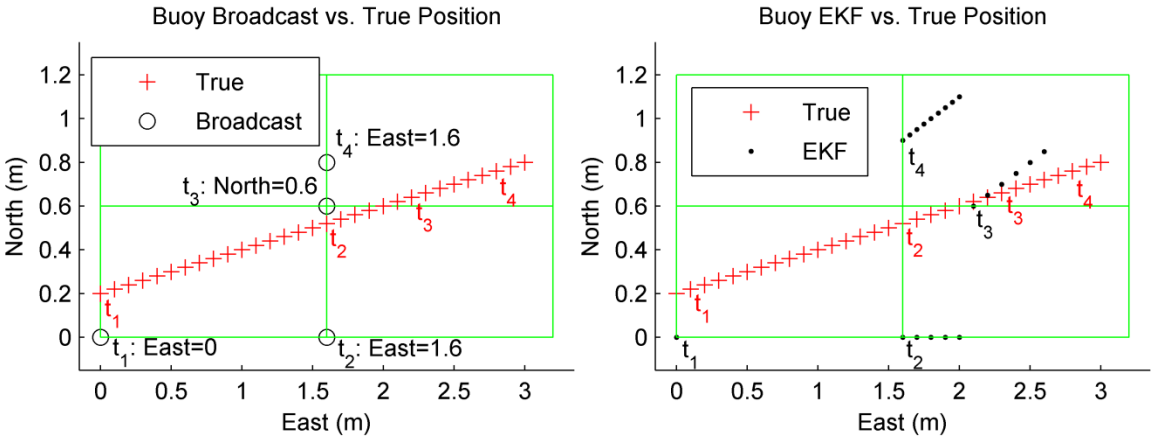

Fig. 7 A comparison between buoy true, broadcast, and EKF positions in a constant linear drift scenario. The green boundaries mark out the bounds of 1.6x0.6 m position quantization. Shown on the left are the messages broadcast at four different times by the floating buoy. Shown on the right is the resulting buoy EKF behavior when the speed and heading states are not fixed

Three potential solutions to this problem with buoy EKF behavior were considered. First, the buoy EKF can be allowed to behave as it does in Fig. 7, modifying the speed and heading according to the position jumps when the buoy crosses a quantization box; although the behavior provides a poor kinematic model of buoy motion, it is still reasonably accurate and simulations have shown that it tends to improve over time. Next, the buoy EKF process noise covariances for speed and heading can be given very small values, corresponding to very high trust in the initialization point (zero speed, arbitrary heading); in this case, the buoy EKF would have near-zero speed for the entire run, with the position estimate jumping discretely between quantization bounds. Finally, there is the option of using finer quantization spacing for the buoy's position measurements. The current quantization scheme was designed with a (relatively) quickly-moving objective ship in mind. The large quantization spacing, combined with the buoy's low drift speeds and lack of speed and heading measurement, make the current quantization method a less-than-optimal fit for buoy position estimation. This option potentially allows for a more accurate real-time position estimate, given its higher-precision position measurements.

Coefficient optimization was performed using a constrained, nonlinear optimization routine using MATLAB®'s '`fmincon`' function, set to use an active-set method. The cost function will be drawn from Monte-Carlo simulation; for AUV EKF coefficients consisted of the mean estimated AUV position error in the measurement zone, and for buoy EKF coefficients it consisted of the mean estimated buoy position error for the entire mission. AUV EKF coefficients were initialized at the values previously used in MSBL navigation, and buoy EKF coefficients were initialized at the corresponding ship EKF values. Constraints used were a lower bound of zero in all cases, and upper bounds shown in Table 2 that correspond to conservatively-estimated upper bounds on the magnitude of expected noise or uncertainty during operation.

TABLE 2. EKF COEFFICIENT OPTIMIZATION CONSTRAINTS: UPPER BOUNDS

Coefficient Matrix	**Corresponding State or Noise Term**			
	East (m^2)	**North (m^2)**	**Speed $(m/s)^2$**	**Heading (rad^2)**
$\boldsymbol{Q}^A$	3	3	--	--
$\boldsymbol{P}^B$	30	30	5	$4\pi^2$
$\boldsymbol{Q}^B$	10	10	5	$4\pi^2$

2.4: HBL Performance Evaluation

The design and implementation cycle of this research can roughly be broken into two main components: testing done in a MATLAB®-based simulation environment, and field testing at a facility on Lake Pend Oreille, Idaho. In the initial design and testing phase of this research, a number of different alternatives were considered before arriving at the current implementation of HBL navigation. Much of the evaluation of these alternatives was done using MATLAB®, and out of that has grown a robust simulation environment. The field testing and simulation verification is supported at a facility operated by the Acoustic Research Detachment (ARD) of the Naval Surface Warfare Center, Carderock Division. It is located on Lake Pend Oreille in Bayview, Idaho.

2.4.1: Simulation

The simulation used to test and evaluate the various components of HBL navigation was designed to represent as accurately as possible the actual proposed testing conditions. The mission layout consists of the high-level parameters of the magnetic signature mission. The mission area has dimensions of 400 m east by 150 m north. The AUV and ship attempt to follow a waypoint path oriented east-to-west, located centrally within the mission area. The two vehicles travel counter-course to one another. Because the system is designed around the use of OWTT communication and ranging, it is expected that multiple AUVs navigating in formation will not change the performance of the system; in the interest of simplicity, the simulation has therefore been designed around missions with only a single AUV.

The buoy is located initially off the path, its initial position seeded randomly within the "optimal effect" area determined by the optimization results. The initial true states for the AUV and ship are randomly distributed around the desired starting state; both vehicles have zero-mean Gaussian noise added to the desired East and North positions, with standard deviations of 4 m. Initial speed and heading are treated likewise, with standard deviations of .05 m/s and .1 rad, respectively. These error levels are also used to initialize the EKF for each vehicle.

Simulation vehicle dynamics are based on previous testing and experience at UI. The objective ship and AUV travel at speeds of approximately 1.30 and 0.85 m/s, respectively. Path control for both vehicles is modeled after the path controller described in section 2.1.1. Heading change at each time step is bounded by measured maximum vehicle performance: at full speed the AUV can turn at a maximum of ~30 deg/s and although the ship is capable of much faster turning, in practice it is controlled by a human operator attempting to closely follow a path and is therefore bounded at 4 deg/s.

The vehicle dynamics of the buoy are slightly less well-known, and required some degree of approximation. Because the buoy is intended to be free-floating, it will drift with the surface currents and wind. These quantities, however, can vary widely; for example, measurements in Monterey Bay

indicate surface velocity rates ranging from ~10-30 cm/s [22] while measurements in the Gulf Stream range as high as 200-250 cm/s [23]. At the Lake Pend Oreille testing facility described in the next section, acoustic position measurements were taken of a semi-constrained floating barge over an entire test day. The result indicated a median drift of drift 7.4 cm/s; after rejecting outliers at greater drift rates than four times the median, the data indicated a mean drift rate of 5.6 cm/s, with a standard deviation of 3.9 cm/s (N=181). Because the simulation is designed to match the conditions of field testing and not the end-user conditions in the ocean, the buoy drift was modeled using the estimated drift rates in Lake Pend Oreille. Drift direction was random, and selected between two cases: linear drift, and large-radius circular drift. Due to the short duration of each mission (typically less than three minutes), these are expected to be good approximations of actual drift conditions.

Measurements taken in the simulation were subject to the same degree of accuracy as those taken in field testing. The speed and heading measurements for the AUV EKF are drawn directly from its true state. The speed measurement is modified by adding zero-mean Gaussian noise with a 5 cm/s standard deviation. The heading measurement is determined using a compass bias condition generated at the start of each mission; the bias consists of a small (sigma = 0.047°) heading error for each heading (rounded to the nearest degree), and describes continuous regions of heading bias such that all measurements in a region will have similar bias values. The buoy and ship position measurements are taken with DGPS accuracy (± 10 cm), but are quantized on broadcast to a resolution of 0.6 m for North position and 1.6 m for East position to model the effects of 13-bit communication. Ship speed and heading measurement are likewise quantized, with resolutions of 0.015625 m/s and 1.40625° respectively.

Communication during the mission occurs at two-second intervals and consists of a pre-designated broadcast order (i.e. the communication cycle). Range measurements upon receipt of communications have a unique distribution of errors. 50% of ranges are slightly longer than the true value and 35% slightly shorter, in both cases varying up to 0.20 m; 5% are very long, with variation

of 5-10 m; and the remaining 10% are dropped entirely. These types of error model the random effects seen in acoustic communications, such as signal bending and surface reflection. The distribution is based on probabilities determined in past field testing at UI [18].

Because the simulation is designed to model the physical system's behavior based on past testing, the information flow in both is similar. Fig. 8 shows the data handling and controls onboard the AUV for both systems; the main difference between the two is that the simulation disregards depth, since the onboard pressure transducer is assumed to be accurate throughout the mission and it is not a component of the AUV EKF. The file structure and computational architecture of the simulation can be found in Appendix C.

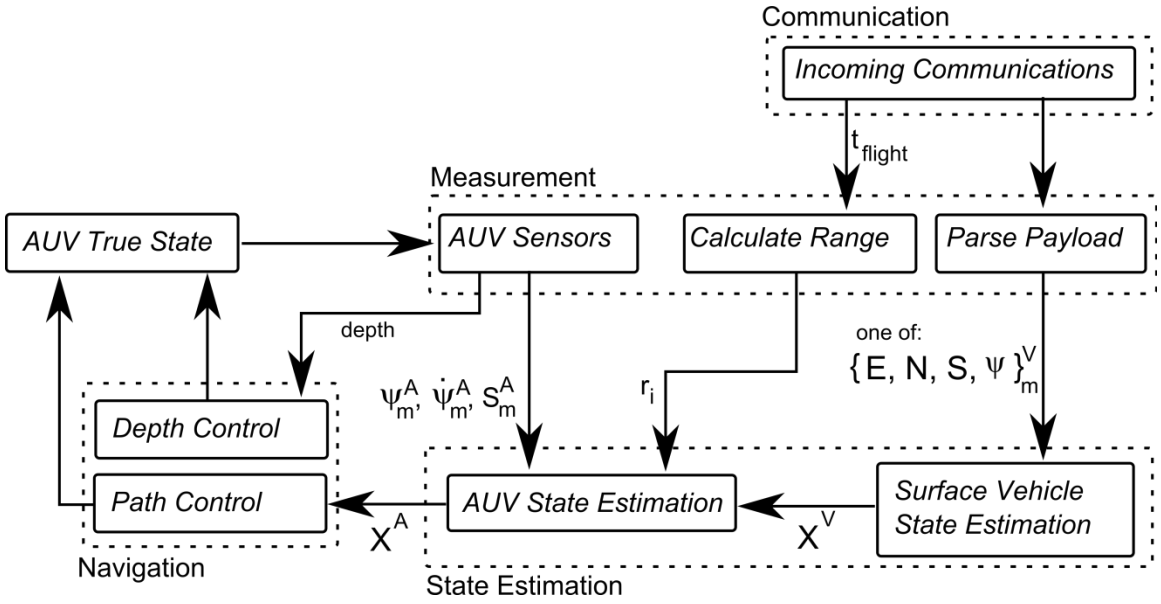

Fig. 8 AUV onboard information flow in HBL navigation. The AUV receives incoming 13-bit messages from the ship and buoy, using them to calculate range to transponder and to update the corresponding surface vehicle EKF. The AUV uses the surface vehicle states and calculated ranges to obtain absolute position measurements, combining those with onboard sensor data in its own EKF. The AUV path and depth controllers rely on the AUV estimated state and measured depth, respectively, for vehicle control.

2.4.2: Field Testing

Verification and testing for this research took place at a barge facility operated by the Acoustic Ressearch Detachment (ARD) of the Naval Surface Warfare Center, Carderock Division in

Bayview, Idaho. The barge, located on Lake Pend Oreille, served as the site for preparation, deployment and monitoring of the AUVs. The magnetic signature mission for HBL navigation followed many of the same operational procedures used in past evaluation of MSBL navigation [7]. Due to the use of OWTT communication and ranging, increasing the size of the AUV fleet does not significantly impact the performance of the system; for ease of operation, field tests performed will therefore be done with only a single AUV.

Fig. 9 The objective ship used in HBL navigation testing, moored to the barge test facility. Shown are the two outriggers supporting the transponders (sides of the ship), one of which is raised, and one of the differential GPS receivers (raised from the bow of the ship) used to acquire ship state data

Each run of the magnetic signature mission consisted of two runs on the AUV: first the AUV was sent on the surface (using GPS to navigate) to a waypoint near the desired start of the mission path; when the objective ship was in place, the AUV began the main mission sequence, diving and driving along the waypoint path counter-course to the ship. The boundaries for the mission define the quantization zone as in the simulation, and constitute an area approximately 400 m by 150 m (East by North). Quantizing East and North position measurements therefore follows the same scheme as has

been previously discussed, with a resolution of 0.6 m in the East direction and 1.6 m in the North direction.

The objective ship used for testing, seen in Fig. 9, is a small vessel equipped with a pair of outriggers on which the two ship-based transponders are mounted. The transponders have a nominal separation of 9.3 m, with a depth of ~1.5 m. The ship additionally has a pair of DGPS receivers mounted bow and stern from which its position, speed and heading are acquired. Its operation during missions is managed by a human pilot, who attempts to maintain a steady 1.3-1.5 m/s and follow the waypoint path shown on a GPS display.

Fig. 10 The experimental floating buoy setup used in HBL navigation. Shown bottom-center are the hardware housing for the WHOI micro-modem. At top left is the DGPS receiver, directly below which is submerged the acoustic transducer. Visible at the building's corner is the tail of the AUV used to control communication and quantize DGPS position data

The floating buoy used to test HBL navigation consisted of an AUV for logic and communications control, an external WHOI micro-modem interfacing with an acoustic transducer, and a GPS unit. Initial testing using standard GPS demonstrated a large error (greater than 10 m) in the buoy location which resulted in poor in-mission AUV navigation. Further examination showed this to be the result of a poor GPS fix, likely caused by overhead structures on the barge in combination with the already-low positional resolution of standard GPS. The issue was addressed by removing the position of the buoy to a more open location and installing a DGPS receiver to increase the accuracy of the position measurement for the buoy. The resulting experimental setup is shown in Fig. 10.

Fig. 11 The independent tracking array used for UI AUV testing, shown relative to the barge facility

In addition to the main system components used for navigation, the testing facility also has an independent tracking system that can be used to determine AUV position to within 10 cm [24]. The tracking system consists of five bottom-mounted transponders, arranged as shown in Fig. 11. The white object shown is the floating barge described above. During missions, pings to the tracking system are "piggy-backed" with other inter-vehicle communications. The tracking system, commonly referred to as "topside" tracking due to its high accuracy and independent measurements, uses a time difference of arrival (TDOA) approach to calculate AUV position at the time of its tracking ping. Because the topside system, AUV fleet, floating buoy and objective ship all utilize clocks synchronized to the same source (GPS), these calculated topside points are used as the comparison data for accuracy results throughout this research.

The choice to collect data using only a single AUV is also related to the piggy-backed topside tracking points. Because the system can only track a single ping at a time, multiple-AUV fleet missions require the vehicles to take turns sending tracking pings. The result of this is that each AUV has a lower density of tracking pings with which to verify the accuracy of its navigation. Use of a single AUV instead of a fleet allows the AUV to send a tracking ping after every message (every two seconds), resulting in a much greater density of tracking pings.

2.4.3: Post-Mission Analysis

During the magnetic signature mission, the AUV uses the estimated positions of the buoy and objective ship in its EKF. When it receives a range from either source, it treats those positions as constants and uses them to update its own position. Due to variations in surface conditions, non-constant surface vehicle motion, and measurement quantization, the estimated positions of the buoy and ship tend to be inaccurate. It is possible, however, to resolve this inaccuracy in postprocessing.

Throughout each run, ship DGPS data is logged prior to quantization. In postprocessing, the AUV EKF can use this information – instead of the estimated positions from the ship EKF – to obtain

higher-accuracy estimates of its own position. With a mean ship EKF position error of 3.49 m [7], this is expected to create significant improvement in localization accuracy.

Determining the most accurate buoy position for postprocessing was somewhat more involved. Due in part to the data handling methods onboard the AUV (an AUV was used in the implementation of the floating buoy), on the final system implementation there were three different conflicting methods for obtaining the buoy position (in addition to the 8-bit quantized value that was broadcast to the AUV during the mission). The first of these is the direct log of DGPS data. It is ideally the best candidate for a postprocessing buoy position, being high-rate and high-accuracy. Unfortunately, this data was not logged during testing and is unavailable for analysis.

The second set of buoy position data is the DGPS record logged onboard the AUV that was used as the buoy during testing. As a result of design decisions made early in the construction and programming of the UI AUV, latitude and longitude information from GPS are stored in floating point variables. On a Rabbit Microcontroller, a floating point has a precision of 32 bits. Because the decimal value of latitude has two significant digits before the decimal (+47°), the maximum accuracy stored onboard the AUV is $4 * 10^{-6}$ degrees. This corresponds to a local resolution of 0.445 m in the north direction. Adding the third digit prior to the decimal for longitude (-116°) reduces the post-decimal bitwise precision by one bit, halving the accuracy; the AUV onboard storage therefore only records longitudinal data to a precision of $8 * 10^{-6}$ degrees, or a local resolution of 0.596 m in the east direction. Although at this point the data was not logged, it was broadcast via radio to researchers during testing and used to evaluate buoy position in real-time. The final logged data shows further decrease in resolution; buoy logs for the test day indicate a local coordinate resolution of 1.137 m East by 0.849 m North, which corresponds neatly to an additional roundoff loss of one bit of precision from the previous floating point resolution. It is likely that this loss occurs during the packet handling process onboard the AUV prior to logging.

The last set of buoy position data is derived from the topside tracking system. At its maximum capability, the AUVs (or buoy) send out a tracking ping once every two seconds –

corresponding to the frequency of acoustic communications, since the tracking pings are piggy-backed on those messages. Because priority was given to the ability to accurately evaluate AUV position, however, the HBL communication cycle was designed such that the buoy would only send one tracking ping per communication cycle. Further decrease of this rate occurs as tracking pings are occasionally lost or missed by one or more tracking transponders. Although accurate (~10 cm accuracy, similar to DGPS), this data set provides a fairly sparse set of data with which to evaluate the buoy position. In final postprocessing, the buoy topside position was used as the most accurate buoy position. Given the low drift rate of the barge-mounted buoy during testing, it was determined that the delay between buoy topside position points would not be as significant a source of error as the quantization seen in the logged DGPS data.

Finally, in addition to postprocessing with the same EKF structure, an additional position filter can be utilized to re-create the path followed by the AUV during a mission. While Kalman filtering is useful in estimating position in the face of inaccurate or conflicting measurements, it tends to produce discontinuities in state estimates when measurements are received. In order to resolve this, past researchers at UI have developed a Rauch-Tung-Striebel (RTS) smoothing filter. The algorithm used is non-causal, operating first forward through the data then backwards. On the forward pass, it behaves the same as the postprocessing EKF except with a dynamic time step; on the backward pass it smoothes the state, using the algorithms described in [25]. This RTS smoother can be used to provide a continuous state estimate useful for reconstructing the magnetic field through which the AUV traveled.

Chapter 3: Results

Results for simulation and field testing are presented in the following sections. In all cases, localization accuracy is reported for a measurement zone defined with respect to the objective ship, measuring 30 meters ahead and 75 meters behind, as shown in Fig. 12. This measurement zone is on the scale of a naval vessel, and represents the area of interest where localization accuracy will affect the reconstruction of the magnetic signature. All error plots shown in this chapter utilize the coordinate system defined in Fig. 12.

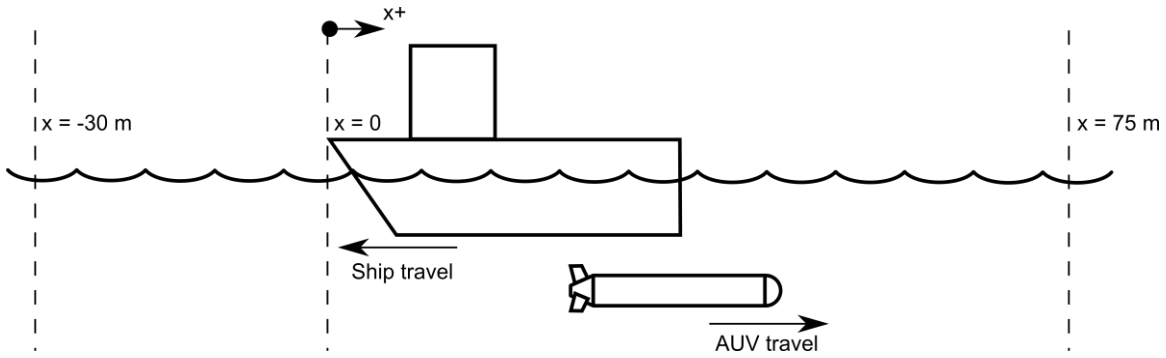

Fig. 12 The magnetic signature measurement zone extends 30 m in front of and 75 m behind the objective ship

3.1: Optimization

3.1.1: Buoy Location Optimization

The results of the buoy location optimization give a clear indication that, as predicted, the geometry of the buoy relative to the AUV-ship waypoint path is a significant factor in HBL navigation. Fig. 13 shows the results of the optimization, with the setup specified previously in section 2.3.1. The error data shown is drawn from a 250-run Monte Carlo simulation at each buoy location; the color indicates the mean error between the estimated and true AUV positions when the buoy is initialized in that grid location.

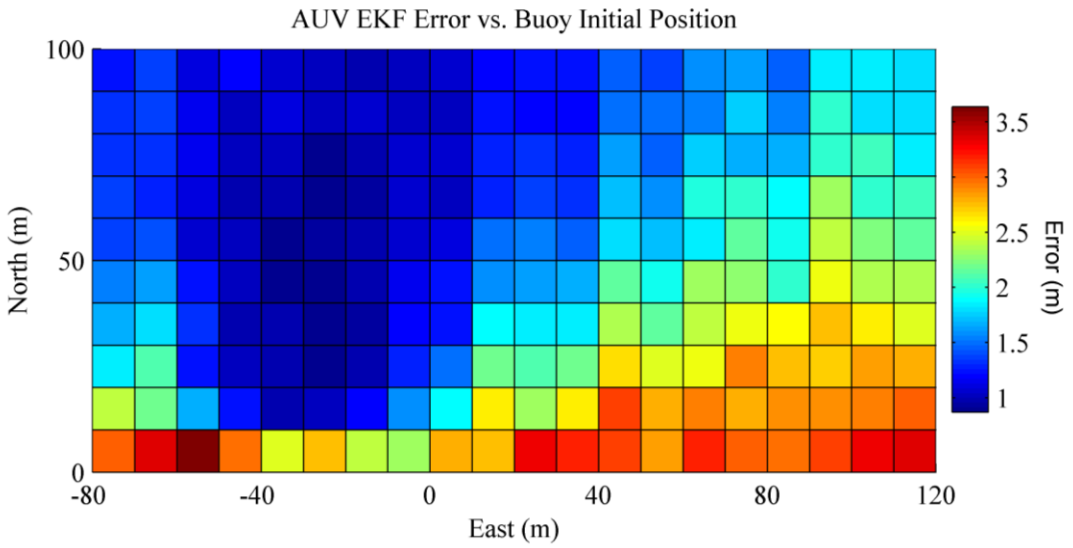

Fig. 13 Results of the buoy location optimization. The mean AUV estimated position error for a Monte Carlo simulation was evaluated with the buoy initialized at each grid location shown. The waypoint path lies along the x-axis with the AUV traveling east. The AUV and ship cross at approximately the origin

An examination of the optimization results shows a clear area in which the buoy is most effective in reducing the position error of the AUV. With the AUV traveling eastward along the x-axis and the ship and AUV crossing at the origin, the buoy is most effective in approximately the region of deepest blue. Further results for this simulation were generated using a buoy position randomly located within this area. Although the buoy drift was set at zero for this optimization, these results can give an indication the performance results for HBL navigation that can be expected of the simulation. HBL navigation (both configurations) is expected to yield ~1-1.5 m AUV position error. Because buoy locations along the waypoint path are qualitatively similar to MSBL navigation, the simulation can be predicted to yield MSBL navigation error of ~3-3.5 m.

3.1.2: Communication Cycle Optimization

Optimization of the communication cycle shows a minimal difference between the two candidates. A 250-run Monte Carlo evaluation of the HBL Short cycle yielded a mean AUV error of 1.37 with a standard deviation of 0.76; the same method for the HBL Long cycle yielded a mean of

1.59 m with a standard deviation of 0.95 m. At p=95%, the true difference between means for the two cycles lies between 0.07 m and 0.37 m. Because the difference is small, the practical utility of the HBL Long cycle is sufficient to bias the optimization in favor of that cycle. The communication cycle selected for the final simulation and field testing results is therefore the HBL Long cycle, shown previously in Table 1.

3.1.3: Buoy EKF Optimization

The buoy EKF optimization was performed in two parts, starting with the optimization of the coefficient matrices. The results, based on simulation data, are given in Table 3. It is worth noting that several of the results are identical to those used in MSBL navigation, as seen in previous work [26]. Although the optimization algorithm did find new local minima for the HBL system, they were not found until the constraints loosened – for example, the East state estimate error covariance $\boldsymbol{P}^B(1,1)$ for the buoy EKF was minimized at approximately 85 m^2, corresponding to a much higher initial position uncertainty than is seen in either simulation or field tests (the initial position error, based on GPS accuracy and drift conditions, is typically less than 5 m). For these values, it was estimated that the maximum initial uncertainty would correspond loosely to the process noise in the ship position states, the measurements for which are derived using the same measurement system (DGPS).

TABLE 3 EKF COEFFICIENT OPTIMIZATION RESULTS

Coefficient Matrix	**Corresponding State or Noise Term**			
	East (m^2)	**North (m^2)**	**Speed $(m/s)^2$**	**Heading (rad^2)**
$\boldsymbol{Q}^A$	0.255448	0.255448	--	--
$\boldsymbol{P}^B$	21.36663	21.36663	0.00016215	0.000001
$\boldsymbol{Q}^B$	0.535915	0.535915	0.00016215	0.000001

It is also worth noting here that the buoy EKF process noise uses a model with a small amount of uncertainty in the speed, and almost none in the heading. In practice, this results in a buoy EKF that will tend to have a low but nonzero velocity, and a heading that almost never changes from the initialization position. Fig. 14 shows three different possibilities for buoy EKF behavior in simulation, the first two of which were discussed in section 2.3.3. The grid lines in the figure correspond to regions of position measurement quantization, providing a good display of how quantization affects the behavior of the buoy EKF.

The initial speculation for the buoy EKF optimization was that it would follow one of the first two trends. Shown in Fig. 14 (left), the first option shows the behavior of a buoy EKF with low trust (high process noise covariance) in the initial speed and heading estimates. In this constant, linear drift simulation, the buoy EKF moves through a wide variety of different speeds and headings and the state estimate better matches the true state as time progresses. Despite this, there remain regions in which there is a large error in estimated position.

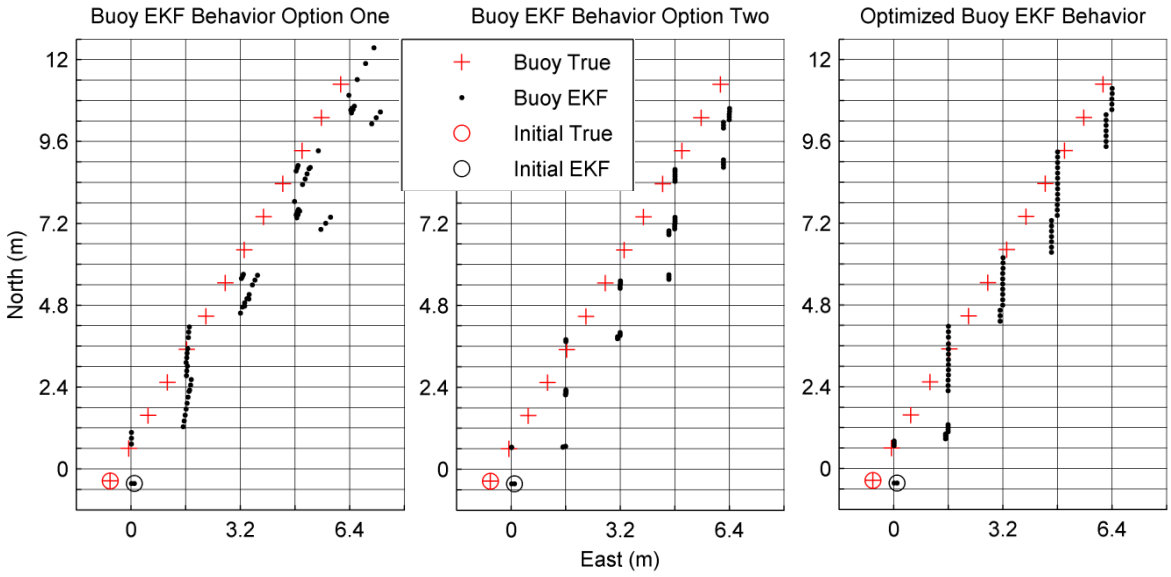

Fig. 14 Buoy EKF behavior in simulation. Shown in order left to right are: EKF behavior with low trust in initial speed and heading; behavior with high trust in initial speed and heading; and optimized behavior. True position markers are 12.5 s apart, and EKF position is displayed every 2 s

The second option, shown in Fig. 14 (center), corresponds to a buoy EKF in which a high trust is given to the initial speed and heading estimates (very low process noise covariance). The EKF

was initialized with a speed state of 0 m/s and a heading of directly north. Throughout the mission the speed changes little, as evidenced by the small drift seen in the EKF position estimate; the heading shows almost no change, as the position estimate drift is continually northward. Although this does not provide a very accurate kinematic model of buoy motion, it is stable and has a very consistent position error.

The optimized result, shown in Fig. 14 (right), is a mix between the first two options. The process noise covariance in speed is comparatively high while the covariance for heading is very low. This allows the position estimate to drift in the north/south direction proportional to the rate of buoy motion in that direction, and the near-constant heading prevents large position error accumulation between measurements, as seen in option one. With these optimized EKF coefficients, the initial heading estimate was selected as directly north due to the finer position measurement resolution in that direction.

TABLE 4. EKF ACCURACY VS. BUOY POSITION QUANTIZATION RESOLUTION

	Quantization Grid Size (East x North), meters					
	1.6 x 0.6 (Standard)	**0.6 x 0.6**	**0.5 x 0.5**	**0.2 x 0.2**	**0.1 x 0.1**	**0.05 x 0.05**
Buoy EKF	0.94 (m)	0.86	0.87	0.92	1.31	2.31
AUV EKF	1.15 (m)	1.13	1.14	1.17	1.31	1.78
Saturation Error	0.00 (m)	0.00	0.00	0.09	1.11	2.96

The second part of buoy EKF optimization was consideration of a finer quantization scheme. For this optimization it was predicted that a higher process noise covariance in the speed and heading states (corresponding to the behavior seen in Fig. 14 (left)) would, when combined with finer grid spacing, allow for a more accurate real-time position estimate of the buoy. In simulation, there was some evidence that this is indeed the case; Table 4 shows the Monte Carlo results of buoy EKF accuracy at several grid sizes (the ship quantization grid remained constant), and the resulting effect on AUV EKF accuracy.

Several things are apparent upon examination of this data. The first is that, as predicted, the buoy EKF tends to improve as the grid resolution grows finer. It is also clear that the accuracy of the AUV position estimate does not improve. Finally, the previous two trends appear to break at very fine buoy measurement grid resolutions. This last result can be explained by considering the relation between quantization resolution, and quantization bounds. As the resolution decreases, the number of available "boxes" remains the same (256 for an 8-bit message); the result is that the quantization bounds are compressed. Because any measurements outside the bounds saturate the quantization, they get broadcast as positions at the boundary – causing large errors in buoy EKF position estimate as the buoy drifts outside the quantization bounds (and corresponding errors in AUV EKF position estimate). This result can be in the saturation error: for coarser grids there is little or no saturation of buoy position broadcasts, but it becomes a much greater problem for fine grids. As a result of this analysis, it was determined that the current quantization resolution (1.6 m East by 0.6 m North), combined with the optimized EKF coefficients, would be used in further simulation and in field testing.

3.2: Simulation

Because HBL navigation is intended to be a direct improvement over MSBL navigation, results from simulation (and later, results from field testing) will be presented as a comparison between MSBL navigation and HBL configurations One (with one ship transponder active) and Two (with both active). All position data will be shifted such that the crossover point of the AUV and objective ship occurs at the origin. Presented single-run results will be shown using the same Monte Carlo randomization seed for all three navigation configurations in order to maximize the relevance of conclusions drawn visually.

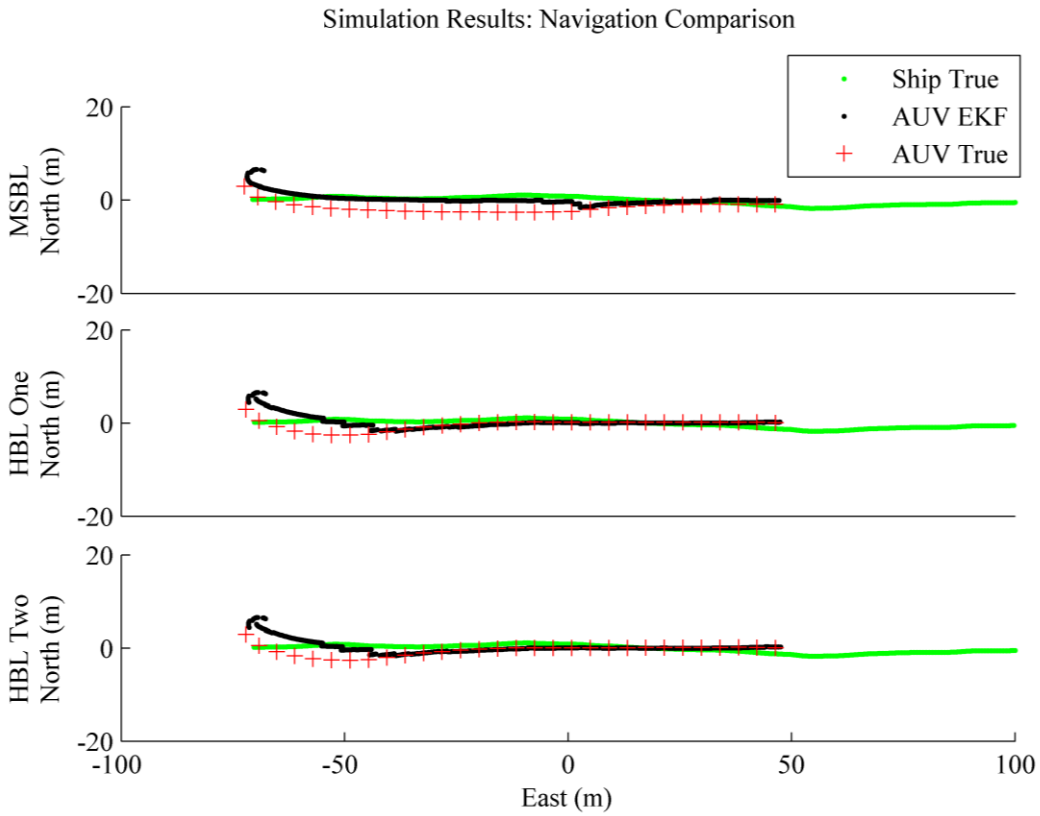

Fig. 15 A comparison of simulation results at each evaluated navigation configuration. The AUV and objective ship cross at approximately the origin, with the AUV traveling to the east

At a run-scale view, the simulation appears to behave as expected, with the AUV navigating toward the path using its estimated position. A representative run for each mission configuration is shown in Fig. 15. In each run, the AUV is traveling to the east and the ship to the west. Ship EKF behavior and buoy EKF behavior are not shown; they both behave as expected (representative simulation buoy EKF behavior can be seen in Fig. 14). Typical EKF behavior can be seen in the lateral jumps in the position estimate; the lateral corrections early in the HBL configurations demonstrate the effects of the buoy on perpendicular-to-path navigation error, in contrast to the lateral jumps near the crossover point (at the origin) in the MSBL mission. Qualitatively, the performances of the two HBL configurations appear very similar to one another.

The localization error results from simulation look similarly promising. Shown Fig. 16 are error magnitude plots from the selected representative runs. The MSBL mission follows closely the previously-demonstrated trend in that navigation method: the AUV quickly corrects its parallel-to-

path error, but the perpendicular-to-path component remains until the AUV approaches the objective ship. The two HBL configurations again demonstrate early corrections in the perpendicular-to-path error, indicating that the buoy is able to successfully reduce the error before the AUV reaches the measurement zone. A 250-run Monte Carlo result yielded a mean error in the AUV position estimate for MSBL navigation of 3.03 m. HBL Configurations One and Two showed mean errors of 1.37 and 1.35 m, respectively.

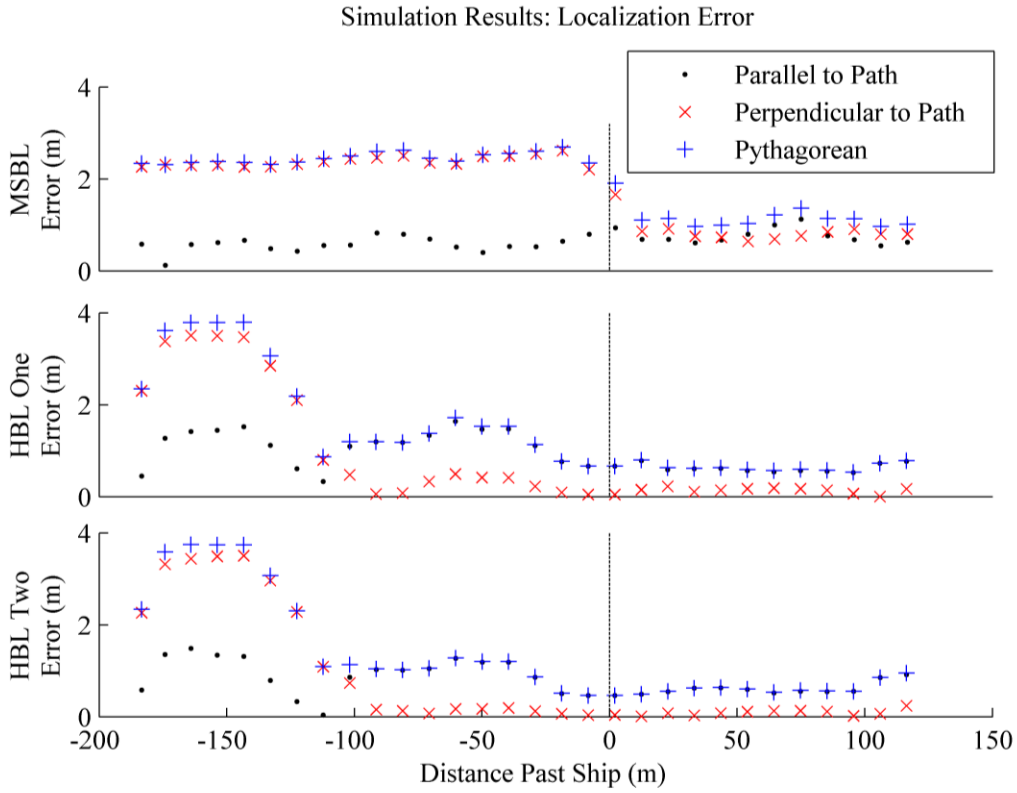

Fig. 16 A visual comparison of error results from simulation. Positions on the negative x-axis indicate that the AUV has not yet passed the ship

3.3: Field Testing

Field test results for HBL navigation were acquired over two separate test dates. MSBL results were acquired previously and are reported here for comparison.. The data displayed in the figures in this section are from the same three test runs: one previously-acquired MSBL run, and one

run each of HBL One and HBL Two configurations. The data displayed are representative of the entire sample, which consists of 24 previous MSBL runs, five runs using the HBL One configuration, and 11 runs using the HBL Two configuration. Because the ship EKF was designed identically to the ship EKF in previous MSBL navigation at UI, and because its performance closely matched that seen in previous results, it will not be shown here. All presented MSBL navigation data and results are drawn from the tests evaluated in [7].

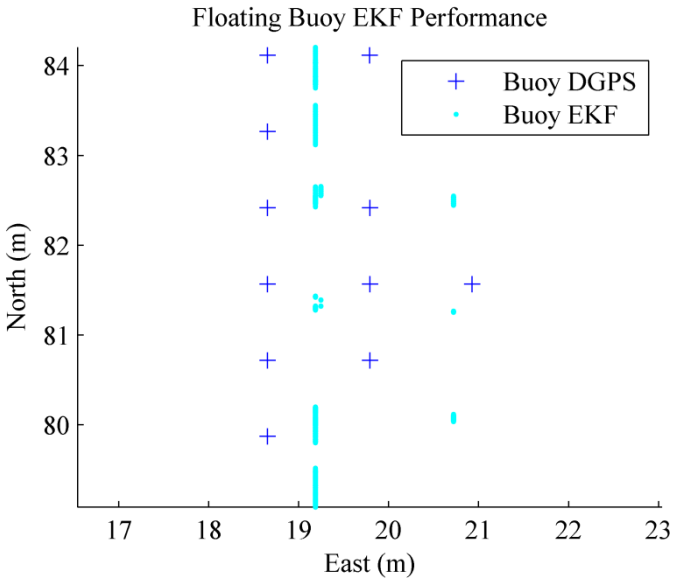

Fig. 17 Field performance of the floating buoy EKF

Fig. 17 shows the in-mission performance of the buoy EKF. The logged position data for the barge-mounted buoy, which drifted in an area approximately 3 m East by 4 m North, is quantized at a resolution of 1.137 m in the East direction and 0.849 m in the North direction. The buoy EKF performance is similar to that seen in simulation, with the initial heading of zero (corresponding to directly North) showing little change throughout the mission. The buoy EKF shows discrete jumps as the buoy moves through quantization boxes, with low resulting speed estimate.

The in-mission navigation results were somewhat mixed, and demonstrated the sensitivity of the system to errors during testing. Fig. 18 shows the results of the onboard AUV EKF during live navigation. As with the presented simulation data, the field test results are normalized such that the

AUV and objective ship cross at approximately the origin, with the AUV traveling east and the ship traveling west. The floating buoy in the HBL runs was located at approximately (20,80); although this is near the limit of the optimal performance area determined in simulation, the buoy is still expected to be effective in this region.

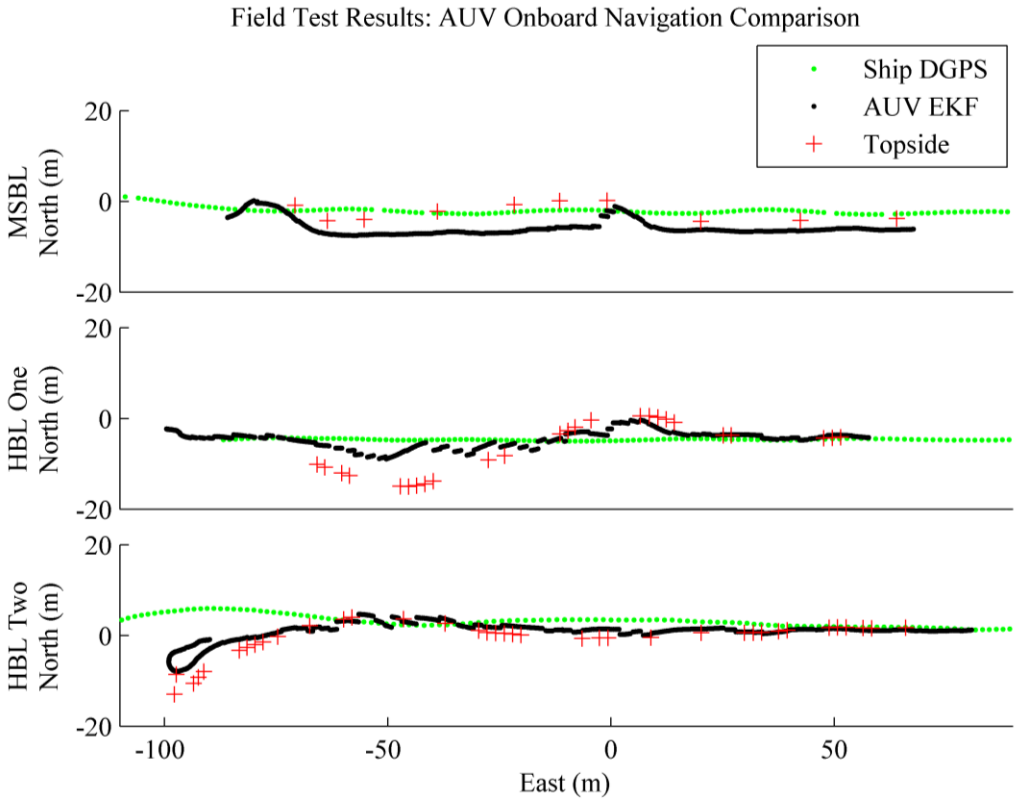

Fig. 18 AUV onboard navigation results from field test runs representative of each navigation configuration. The AUV and objective ship cross at approximately the origin in each run, with the AUV traveling east and the ship traveling west. The floating buoy is located at approximately (20,80) in both HBL runs

Examination of the test results shows behavior similar to that expected. The MSBL navigation run demonstrates a perpendicular-to-path offset early in the run, making lateral corrections as the AUV passes the ship. The HBL One position estimate shows a large, and apparently increasing, error early in the run. As previously mentioned, there were some errors during testing: a boot-up error on the AUV used to collect HBL One data caused it to log and evaluate range data with a two-second delay; and one of the EKF speed coefficients was programmed incorrectly, resulting in large errors

for AUV estimated speed. The HBL Two navigation was much better, showing an apparent lateral position correction early in the run that is maintained as the AUV passes the objective ship.

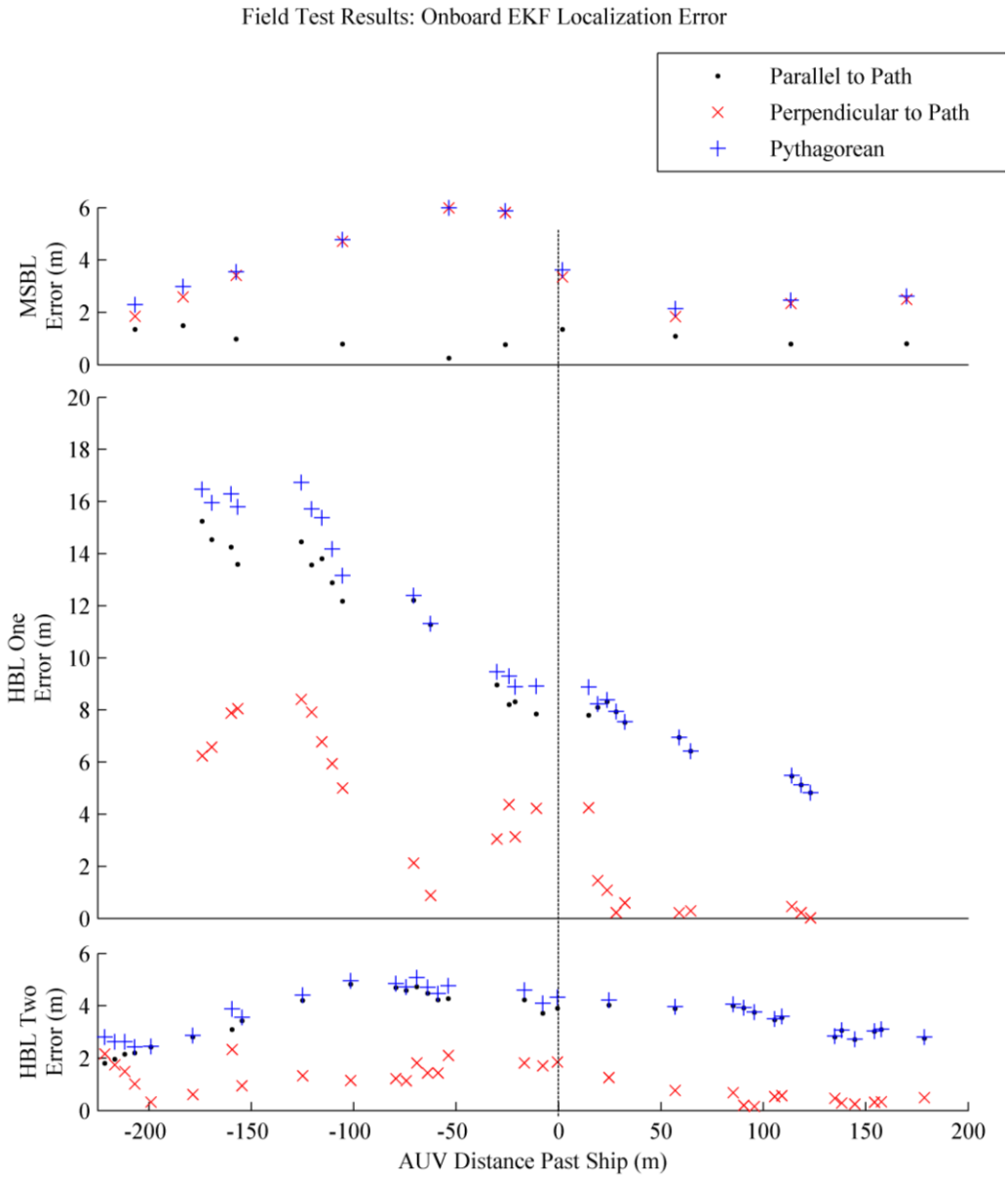

Fig. 19 Error data for AUV navigation in field testing. Positions on the negative x-axis indicate that the AUV has not yet passed the objective ship

Further details of the field test results of navigation can be seen in a breakdown of the position error throughout the run, shown in Fig. 19. The MSBL navigation demonstrates clearly the lateral position corrections shown in the representative run. The HBL One navigation shows a very

high parallel-to-path position error, indicative of the errors described above. These two errors were significant contributors to the large parallel-to-path error seen in both of the presented HBL runs. The perpendicular-to-path error on both of the HBL runs is much better than the parallel-to-path error. The HBL Two data shows a similar trend to that seen in HBL One navigation, though with lower parallel-to-path position error.

3.4: Localization in Postprocessing

The postprocessed results shown are from the same runs seen in the field testing results, and are shifted similarly such that the AUV and objective ship cross at approximately the origin. Fig. 20 shows the localization results of the AUV navigation EKF using the best available measurements of true ship and buoy positions.

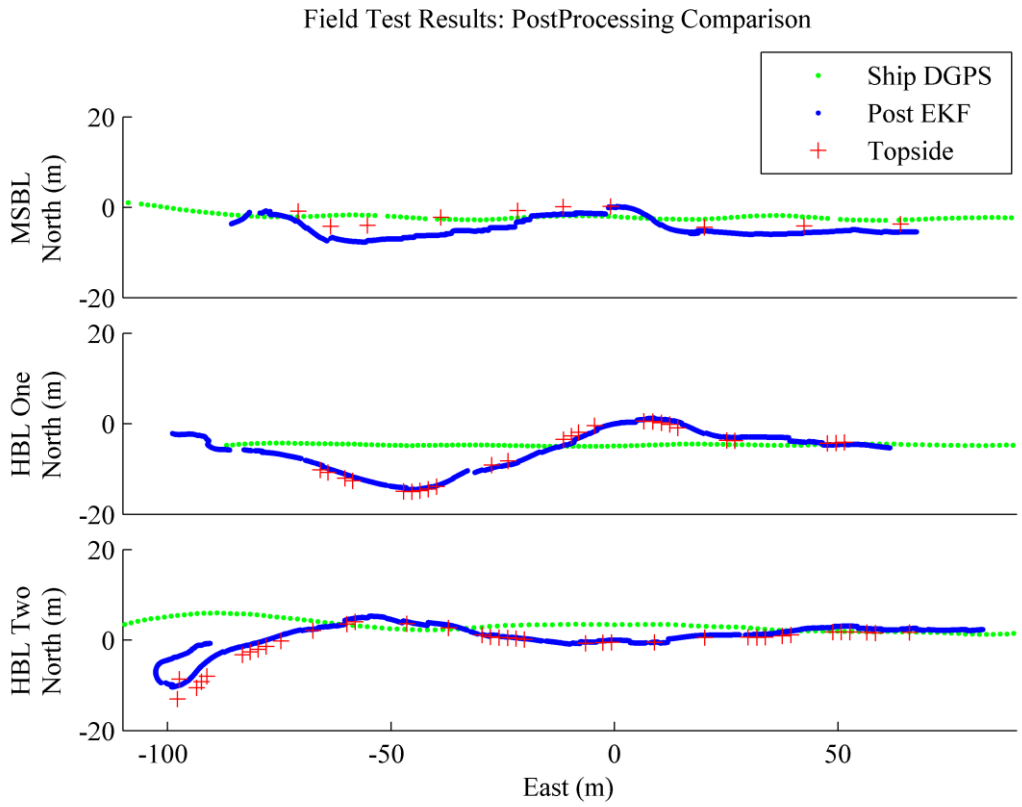

Fig. 20 AUV position results after postprocessing using the best available position data for the objective ship and floating buoy

Due to the previously-discussed quantization of logged DGPS data on the buoy, the best estimate for its position was determined to be the measurements taken by the topside tracking system. The data after postprocessing shows a much-improved error in the estimated AUV position. As with previous results, the MSBL navigation shows improvement as the AUV approaches the objective ship. Both HBL configurations demonstrate early correction in the perpendicular-to-path position, and maintain this accuracy throughout the mission.

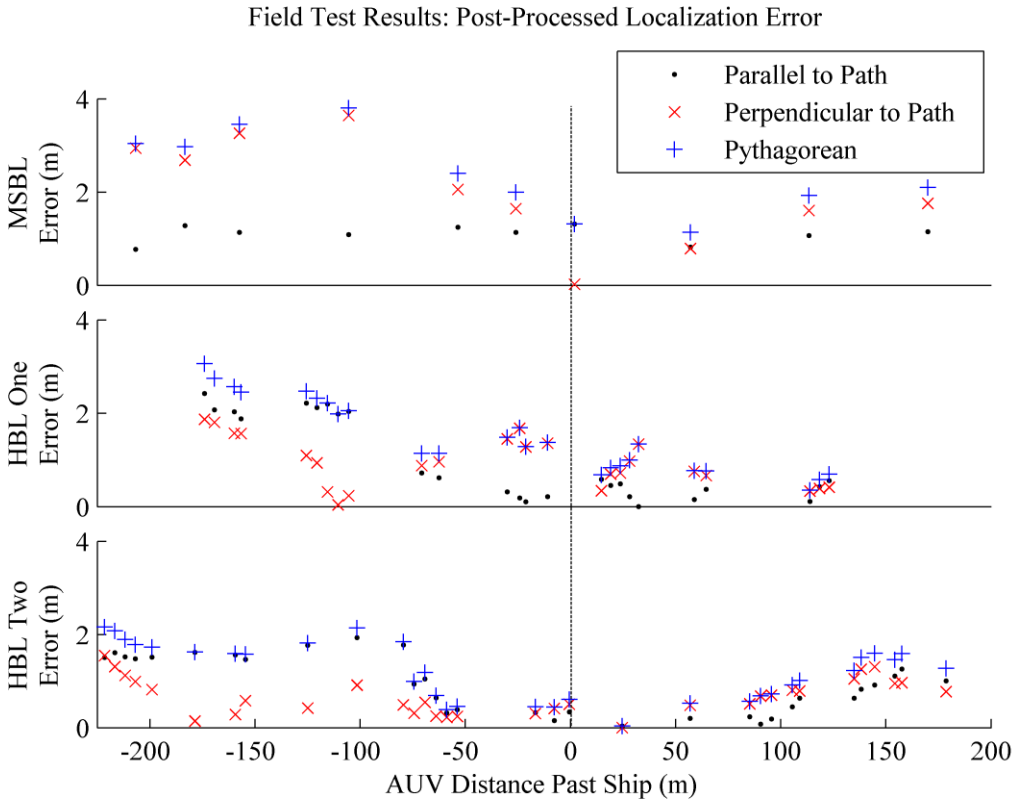

Fig. 21 Error data for AUV navigation after postprocessing with the best available data for objective ship and floating buoy position. Positions on the negative x-axis indicate that the AUV has not yet passed the objective ship

Fig. 21 further demonstrates this result, showing the magnitude of the estimated AUV position error. In particular, the HBL Two configuration shows a high degree of improvement before the AUV enters the measurement zone (30 m prior to passing the objective ship), maintaining this accuracy until the AUV leaves the measurement zone.

Fig. 22 demonstrates the magnitude of improvement between onboard and postprocessed EKF position accuracy. Particularly significant is the accuracy improvement in both HBL configurations. As discussed previously, this is largely due to correction of the onboard EKF speed estimate and the timing error in the WHOI modem.

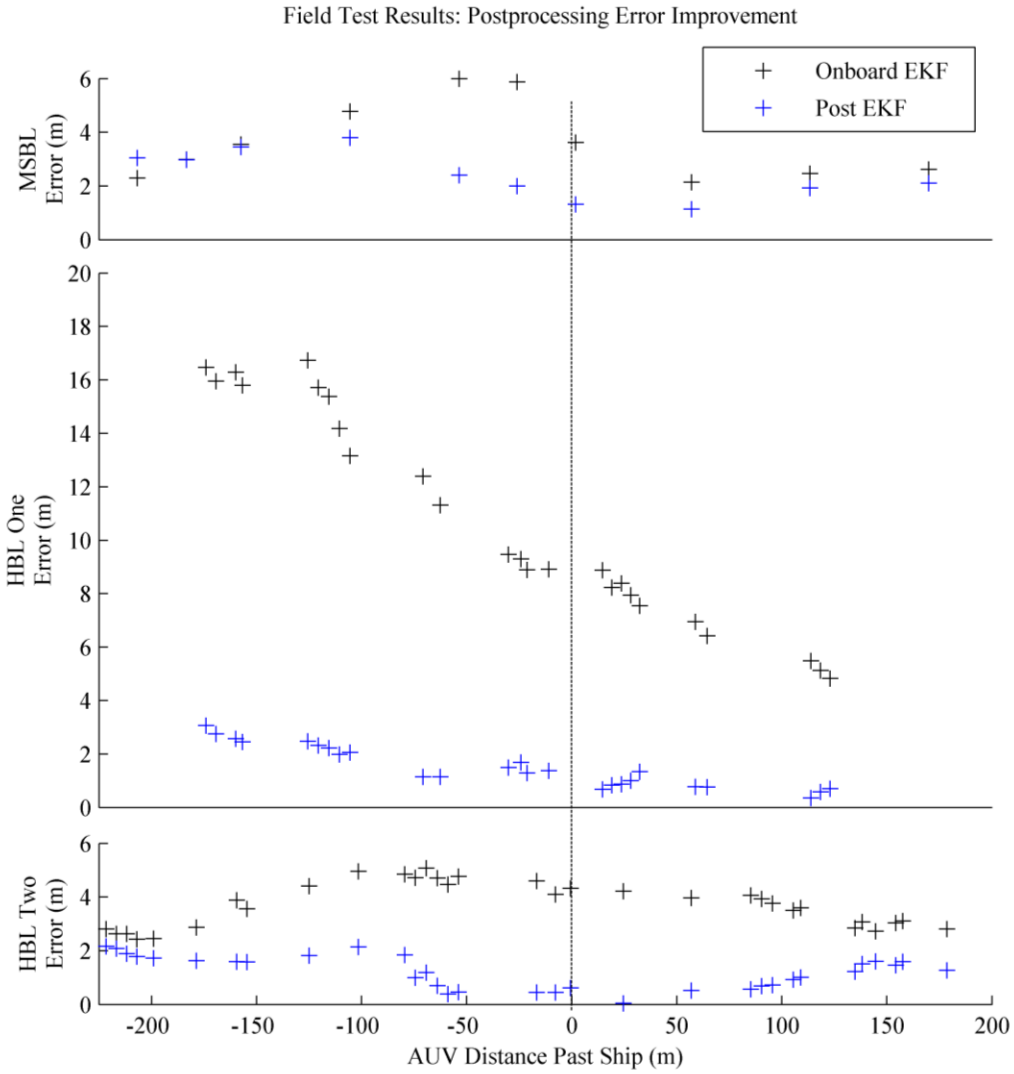

Fig. 22 A comparison between AUV onboard EKF position error and the position error of the postprocessing EKF

The last element of postprocessing is the RTS smoothing algorithm. Because this position estimation method is drawn directly from the postprocessed position data, it is not expected to significantly change the accuracy of the results. Instead, it is intended to provide a more continuous

AUV position, useful when re-creating the magnetic field of the objective ship from the collected magnetometer data. Fig. 23 shows a typical RTS-smoothed result, using the above-shown HBL Two navigation data. The result is a continuous estimate of AUV position, with performance characteristics similar to the postprocessed navigation from which it is derived.

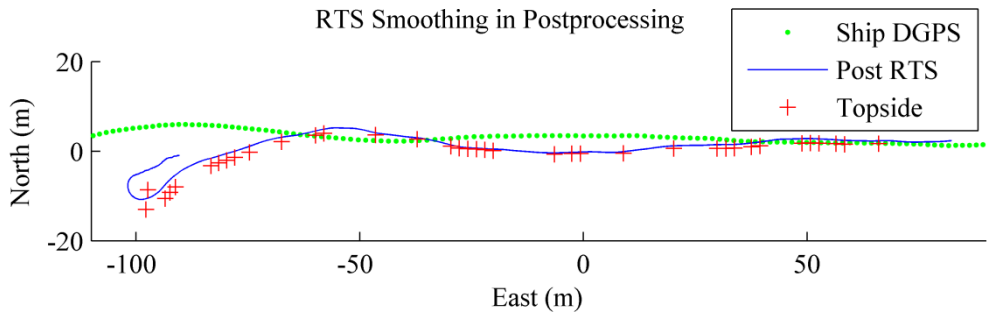

Fig. 23 AUV position in HBL Two navigation after RTS smoothing on the postprocessed AUV EKF position

The final accuracy results of the navigation methods described are shown in Table 5. Although the removal of one ship-mounted transponder between HBL configurations Two and One appears to cause a reduction in AUV localization accuracy, both configurations demonstrate a clear improvement over MSBL navigation. The best result seen out of all HBL tests showed an AUV position error of 0.57 m in the measurement zone.

TABLE 5. AUV ESTIMATED POSITION ACCURACY RESULTS

Navigation Configuration	**AUV Localization Error Evaluation Method**	
	Simulation	**Field Testing**
MSBL	3.03 (m)	3.30
HBL 1	1.37	1.90
HBL 2	1.35	1.59

Chapter 4: Discussion and Conclusions

The methods and results presented in this research demonstrate a novel extension of past AUV navigation methods used in research at UI. The HBL navigation system for magnetic signature missions consists of using an EKF to estimate the AUV position. The EKF is updated with onboard sensor data (speed, heading, and heading rate of change), as well as absolute position measurements of the AUV that are derived from acoustic ranges. The acoustic range sources consist of one or two transponders mounted on the objective ship, as well as one transponder on a buoy floating off the waypoint path. The use of the WHOI micro-modem to communicate synchronously allows the approach demonstrated to be extended to simultaneous AUV fleet operation without significant impact to the length of the communication cycle or the accuracy of navigation.

4.1: HBL Simulation

The design, prototyping, optimization and initial analysis of this system were performed in a MATLAB-based simulation environment. The simulation was designed to closely match the conditions seen in field testing, with noise and error conditions derived from past experimental results using the UI AUVs. The simulation has shown to be an effective method for developing and evaluating new methods of acoustic range-based AUV navigation. The EKFs used in simulation showed similar qualitative behavior to those used onboard the AUV in field testing, matching well with both past MSBL results and newly-acquired HBL results. The simulation was further used to optimize several aspects of HBL navigation relating to buoy location and AUV and buoy EKF behavior. The buoy location was determined to be optimally effective in a fairly large area. This demonstrates a reasonable amount of flexibility in buoy placement and allows for effective navigation under a wide range of drift conditions.

The overall error results seen in simulation were consistently smaller than those seen in field testing in the defined measurement zone. This indicates that there is room for improvement in the

simulation model; it is likely that more accurate noise and error models could be generated and used to improve the accuracy of simulation results. Despite this discrepancy, the error trend seen in simulation matches well with that seen in field tests: both HBL configurations were predicted to show significant improvement over MSBL navigation. The simulation further proved its usefulness when evaluating errors found in early HBL field tests. The use of GPS instead of DGPS for the buoy position, for example, resulted in a ~10 m offset of buoy position and caused very poor navigation on the AUV. Running the simulation with a similar buoy offset condition caused a similar error in AUV navigation, which helped to verify that the buoy offset position was indeed the source of the error and that a more accurate position measurement method would be needed in future tests.

4.2: Floating Buoy Position Estimation

Estimating the position of the floating buoy was an interesting challenge throughout this research. With position measurements quantized for the 13-bit acoustic message, the buoy EKF effectively had a measurement resolution of 1.6 m East by 0.6 m North. At low drift speeds, this coarse resolution proved to be an obstacle to accurate buoy position modeling when using an EKF. Optimization of the EKF coefficients resulted in behavior that resolves this issue by ignoring heading (it stays at approximately the initialization value) and adopting a one-dimensional speed that roughly tracks the buoy position as it drifts through the WHOI message quantization bounds.

Although it is possible to design a buoy such that it can measure and broadcast its speed and heading state, thereby avoiding this difficulty, one of the design goals for HBL navigation was to increase accuracy without significant complexity increases. As it stands, the buoy design requires only a GPS receiver, a processor to quantize the GPS signal at a specified resolution, and a WHOI micro-modem (and acoustic transducer) to broadcast the signal.

4.3: AUV Localization

During real-time navigation, the AUV onboard field test data exhibited a large variance in localization error. In particular, the run data collected for HBL One navigation shows a high degree of sensitivity in timing errors. The exact cause of the error is unknown, but in the HBL One run shown in Chapter 3 the AUV had a timing error in which data received via the WHOI micro-modem (i.e. acoustic messages) was not sent to the rest of the AUV until after a two-second delay. The size of the delay was verified by comparing the logs of the ship, AUV and buoy and matching the timestamps of several outgoing or incoming messages. The end result was poor navigation during field tests. This was further compounded by a programming error in the onboard EKF which resulted in poor speed estimation.

After repairing the testing errors and using accurate surface vehicle measurements, in postprocessing the accuracy of the AUV position estimate greatly improves. The improvements were primarily due to corrections made to the timing of data handling and the accuracy of surface vehicle localization. The postprocessed AUV position data also agrees with the original hypothesis of HBL navigation: the presence of an off-path acoustic ranging source eliminates, to a large degree, the perpendicular-to-path AUV position uncertainty and error seen early in the mission as a result of the transponder geometry in MSBL navigation. Although the mean error over the course of all HBL data collected does not meet the accuracy specification of the project goal there were several individual runs that showed a mean error magnitude in the measurement zone of under 70 cm, well below the target of 1 m. The results from individual runs demonstrate that the desired level of accuracy is within the capability of the current navigation system.

4.4: Future Work

The field test results showed a significant difference between the HBL One and HBL Two configurations, when the simulation predicted minimal difference. Further testing may be necessary difficult to discern the exact cause of this discrepancy, since none of the HBL One runs were error-free during testing. On one test day, the buoy GPS showed a large position offset (compared to the topside tracking position), causing poor navigation throughout all HBL One tests; on the other test day, the AUV selected to test the HBL One configuration had a timing error that was not discovered until later. Further testing is therefore required to accurately evaluate the success of HBL One navigation. Improvements can be made by addressing the previously-discussed GPS data handling issues onboard the AUV, thereby providing a better buoy position estimate in postprocessing.

The results from postprocessing indicate two primary bottlenecks in the accuracy of live navigation using the HBL system: the objective ship EKF and the floating buoy EKF. Improvements to the accuracy of the estimated surface vehicle positions are likely to significantly improve the performance of the AUV during the mission. Because the objective ship (ideally) follows a somewhat predictable path and has reasonably consistent motion throughout the mission, an EKF is well-suited to estimating its position. The inaccuracy in the ship EKF is likely the result of a combination of two main factors: the small size of the vessel used in testing lends to quicker turning, more variable speed, and less steady motion (it is affected by wind and waves) than a large vessel; and the low frequency of updates for any given state. It is likely that tests using a larger objective ship will see less variation in the true course of the ship over the duration of a magnetic signature mission, and that the EKF will have better performance as a result.

In simulation, the use of an EKF for the buoy proved to be a good choice. The constant (or near-constant) drift condition in the simulation was designed to model short-term, unconstrained drift conditions in the ocean. Without constraints, the buoy state will likely remain relatively steady over the course of a ~3-minute mission; this gives the buoy EKF time to estimate the un-measured state values of speed and heading, and eventually arrive at a good estimate of the buoy state. Improvement

in this area, for this type of ocean test, will likely come from implementing a finer quantization grid for buoy position measurements. Although simulation results demonstrated that too fine a grid would result in worse AUV navigation as the buoy drifted out of the grid boundary, it is possible to slightly increase the complexity of the communication cycle and add an additional broadcast specifying the origin of the quantization zone. This allows for a moving zone that can be used to have better position resolution for the buoy EKF. This option likely requires either a more complex (and therefore longer) communication cycle, or a separate method of calculating the location of the current quantization boundaries.

Under actual test conditions, the use of an EKF for the buoy demonstrated to be a poor choice. The constrained drift of the barge facility caused unpredictable drift behavior as the wind, waves, current, and mooring chains interacted. This resulted in a poor predictive model for the state of the floating buoy. Aside from a higher-resolution quantization zone, it may be worth considering alternate types of position estimators if this facility is to be used in future tests as a stand-in for the floating buoy. One possibility is to augment the EKF with a pre-filter state estimator for speed and heading that develops a kinematic model (or just estimates state values) based on the entire past history of buoy position measurements. Alternately, of course, an actual drifting buoy could be designed and constructed, allowing data collection of actual drift conditions and more accurate modeling prior to field testing.

References

[1] J. J. Holmes, *Exploitation of a Ship's Magnetic Field Signatures*: Morgan & Claypool Publishers, 2006.

[2] J. J. Holmes, *Modeling a Ship's Ferromagnetic Signatures*, Morgan & Claypool Publishers, 2007.

[3] H. P. Tan *et al.*, "A survey of techniques and challenges in underwater localization," *Ocean Engineering,* vol. 38, no. 14, pp. 1663-1676, 2011.

[4] P. Baccou, and B. Jouvencel, "Homing and navigation using one transponder for AUV, postprocessing comparisons results with long base-line navigation." pp. 4004-4009.

[5] J. Leonard, and P. Newman, "Pure range-only sub-sea SLAM," in IEEE International Conference on Robotics and Automation, Taipei, 2003.

[6] J. Feusi *et al.*, "Comparison of independently-moving transponder configurations for AUV fleet navigatoin with one-way acoustic ranging," in IEEE Oceans, Hampton Roads, 2012.

[7] E. Wolbrecht *et al.*, "Field testing of moving short-baseline navigation for autonomous underwater vehicles using synchronized acoustic messaging," *Journal of Field Robotics,* vol. 30, no. 4, pp. 519-535, 2013.

[8] N. H. Kussat, C. D. Chadwell, and R. Zimmerman, "Absolute positioning of an autonomous underwater vehicle using GPS and acoustic measurements," *IEEE Journal of Oceanic Engineering,* vol. 30, no. 1, pp. 153-164, 2005.

[9] P. A. Miller *et al.*, "Autonomous underwater vehicle navigation," *IEEE Journal of Oceanic Engineering,* vol. 35, no. 3, pp. 663-678, 2010.

[10] B. Armstrong *et al.*, "Field measurement of surface ship magnetic signature using multiple AUVs."

[11] S. Smith, and D. Kronen, "Experimental results of an inexpensive short baseline acoustic positioning system for AUV navigation." pp. 714-720.

[12] M. Morgado, P. Oliveira, and C. Silvestre, "Tightly coupled ultrashort baseline and inertial navigation system for underwater vehicles: An experimental validation," *Journal of Field Robotics,* vol. 30, no. 1, pp. 142-170, 2013.

[13] D. J. Stilwell *et al.*, "Design elements of a small low-cost autonomous underwater vehicle for field experiments in multi-vehicle coordination."

[14] G. Beidler, and R. Wall, "Low cost distributed control system for autonomous Vehicles."

[15] P. M. Newman, *MOOS-mission orientated operating suite*, Dept. of Ocean Engineering, Massachusets Institute of Technology, Cambridge, MA, USA, 2006.

[16] L. Freitag *et al.*, "The WHOI micro-modem: an acoustic communications and navigation system for multiple platforms." pp. 1086-1092.

[17] M. F. Fallon *et al.*, "Cooperative AUV navigation using a single maneuvering surface craft," *The International Journal of Robotics Research,* vol. 29, no. 12, pp. 1461-1474, 2010.

[18] J. R. Canning *et al.*, “A low bandwidth acoustic communication strategy for supporting collaborative behaviors in a fleet of autonomous underwater vehicles,” *US Navy Journal of Underwater Acoustics,* vol. 59, no. 3, 2009.

[19] B. P. Crosbie *et al.*, "Synchronous navigation of AUVs using WHOI micro-modem 13-bit communications."

[20] D. Simon, *Optimal state estimation: Kalman, H infinity and nonlinear approaches*: Wiley-Interscience, 2006.

[21] B. Armstrong, E. Wolbrecht, and D. Edwards, "AUV navigation in the presence of a magnetic disturbance with an extended Kalman filter."

[22] J. Paduan, and L. Rosenfeld, “Remotely sensed surface currents in Monterey Bay from shore-based HF radar (Coastal Ocean Dynamics Application Radar),” *Journal of Geophysical Research,* vol. 101, no. C9, pp. 20669-20686, 1996.

[23] D. E. Barrick, M. W. Evans, and B. L. Weber, “Ocean Surface Currents Mapped by Radar,” *Science,* vol. 198, no. 4313, pp. 138-144, 1977.

[24] D. Odell *et al.*, "A versatile tracking system for AUV testing."

[25] S. Sarkka, “Unscented Rauch-Tung-Striebel Smoother,” *IEEE Transactions on Automatic Control,* vol. 53, no. 3, 2008.

[26] J. Stringfield, “Navigation and Localization of an Autonomous Underwater Vehicle Fleet for Magnetic Field Measurements,” University of Idaho, Moscow, Idaho, 2012.

Appendix A: The Extend Kalman Filter

Extended Kalman filtering work in this research is based on the presentation of the filter in [20].

The extended Kalman filter (EKF) utilizes a nonlinear state propagation model $\boldsymbol{f}$ that predicts the current state $\boldsymbol{x}_k$ based on the previous state $\boldsymbol{x}_{k-1}$, control inputs $\boldsymbol{u}_{k-1}$,and process noise $\boldsymbol{w}_{k-1}$ with

$$\boldsymbol{x}_k = \boldsymbol{f}_{k-1}(\boldsymbol{x}_{k-1}, \boldsymbol{u}_{k-1}, \boldsymbol{w}_{k-1}),$$

where *k* indicates the time step. The process noise is zero-mean and Gaussian, with a known variance. The covariance of the process noise is defined by the coefficient matrix $\boldsymbol{Q}_k$.

The nonlinear measurement update model $\boldsymbol{h}_k$ predicts measurement values $\boldsymbol{z}_k$ using the current state and measurement noise $\boldsymbol{v}_k$ with

$$\boldsymbol{z}_k = \boldsymbol{h}_k(\boldsymbol{x}_k, \boldsymbol{v}_k).$$

The measurement noise is likewise zero-mean and Gaussian, with known variance. The covariance of the measurement noise is defined by the coefficient matrix $\boldsymbol{R}_k$. In this research, the process and measurement noise covariances remain constant throughout filter operation: $\boldsymbol{Q}_k = \boldsymbol{Q}$ and $\boldsymbol{R}_k = \boldsymbol{R}$. Further, the matrices $\boldsymbol{Q}$ and $\boldsymbol{R}$ are defined as diagonal, indicating that the noise terms in the system behave independently of one another. For example, the noise in an East position measurement is independent of the noise in the previous North position measurement.

The EKF is initialized with expected initial state $\boldsymbol{x}_0$, with initial state estimate error covariance $\boldsymbol{P}_0$ defined as the expected error between the actual and estimated initial states. Filter operation takes place in two steps: predict and update, with the state after each step described as *a priori* ($\boldsymbol{x}_k^-$) or *a posteriori* ($\boldsymbol{x}_k^+$), respectively. The EKF iterates through discrete time steps for $k = 1, \ldots, N$.

During the predict step, the state model is linearized about the previous state point using the Jacobians

$$\boldsymbol{F}_{k-1,ij} = \left.\frac{\partial \boldsymbol{f}_{k-1}(\boldsymbol{x},\boldsymbol{u},0)_i}{\partial \boldsymbol{x}_j}\right|_{\boldsymbol{x}_{k-1}^{+}}$$

and

$$\boldsymbol{W}_{k-1,ij} = \left.\frac{\partial f_{k-1}(\boldsymbol{x},\boldsymbol{u},\boldsymbol{w})_i}{\partial \boldsymbol{w}_j}\right|_{\boldsymbol{x}_{k-1}^{+}}$$

The predicted *a priori* state is determined using the state propagation model with the assumption of zero noise, based on the previous *a posteriori* state with

$$\boldsymbol{x}_k^{-} = \boldsymbol{f}_{k-1}(\boldsymbol{x}_{k-1}^{+}, \boldsymbol{u}_{k-1}, \boldsymbol{0}).$$

The *a priori* state estimate error covariance is updated based on the previous linearizations, the previous *a posteriori* state estimate error covariance, and the previous measurement noise covariance using

$$\boldsymbol{P}_k^{-} = \boldsymbol{F}_{k-1}\boldsymbol{P}_{k-1}^{+}\boldsymbol{F}_{k-1}^{T} + \boldsymbol{W}_{k-1}\boldsymbol{Q}\boldsymbol{W}_{k-1}^{T}.$$

The update step occurs immediately following the predict step and begins similarly with two linearizations, using the Jacobians

$$\boldsymbol{H}_{k,ij} = \left.\frac{\partial \boldsymbol{h}_k(\boldsymbol{x},0)_i}{\partial \boldsymbol{x}_j}\right|_{\boldsymbol{x}_k^{-}}$$

and

$$\boldsymbol{V}_{k,ij} = \left.\frac{\partial \boldsymbol{h}_k(\boldsymbol{x},\boldsymbol{v})_i}{\partial \boldsymbol{v}_j}\right|_{\boldsymbol{x}_k^{-}}$$

The update gain matrix $\boldsymbol{K}_k$ is calculated with

$$\boldsymbol{K}_k = \left(\boldsymbol{P}_k^{-}\boldsymbol{H}_k^{T}\right)\left(\boldsymbol{H}_k\boldsymbol{P}_k^{-}\boldsymbol{H}_k^{T} + \boldsymbol{V}_k\boldsymbol{R}\boldsymbol{V}_k^{T}\right)^{-1}.$$

The update step proceeds by calculating the current *a posteriori* state based on the residual error between the measurement and the predicted measurement using

$$\boldsymbol{x}_k^{+} = \boldsymbol{x}_k^{-} + \boldsymbol{K}_k * \left(\boldsymbol{z}_k - \boldsymbol{h}(\boldsymbol{x}_k^{-}, \boldsymbol{0})\right)$$

And concludes by generating the *a posteriori* state error covariance matrix with

$$\boldsymbol{P}_k^+ = (\boldsymbol{I} - \boldsymbol{K}_k \boldsymbol{H}_k)\boldsymbol{P}_k^-.$$

It is worth noting that in the case that a given measurement is not available for the current time step, the measurement vector $\boldsymbol{z}_k$ is undefined at the index of that measurement. The measurement vector, update model and corresponding noise covariance matrices may therefore reduced at that time step by eliminating the corresponding entries from calculations.

In the case that no measurement at all is available for the current time step, the update model reduces to

$$\boldsymbol{x}_k^+ = \boldsymbol{x}_k^-$$

and

$$\boldsymbol{P}_k^+ = \boldsymbol{I}\boldsymbol{P}_k^- = \boldsymbol{P}_k^-.$$

Computational efficiency may therefore be increased by neglecting the update step except when a measurement has occurred.

Appendix B: The 13-bit Acoustic Message Structure

One of the available transmission modes for the WHOI micro-modem enables the broadcast and receipt of 13-bit acoustic messages. In addition to a string at the start of the packet indicating whether the packet is being sent or received ($CAMUC and $CAMUA, respectively), each packet takes the form

SRC,DEST,HHHH*CS

SRC and **DEST** are the modem identification numbers of the source and destination modems, respectively. In research at UI, the **DEST** field is typically given a value of 0 indicating that the message is intended to be received by all listening WHOI modems. In HBL navigation missions, the **SRC** field is specified using the convention: 13 for floating buoy, 14 for ship port, 15 for ship starboard.

The **HHHH** field contains the 13-bit payload, encoded by the modem as a hexadecimal string. In most magnetic signature mission research at UI, the first two entries (the first five bits) are used to designate the type of message being sent. Relevant to HBL research are the following:

1A NORTH
1B EAST
1C SPEED
1D HEADING
1F ABORT

The trailing two hexadecimal digits (the last eight bits) of the message contain the payload, which in this research is typically the index (0-255) for the quantization “box” in which the corresponding measurement is located.

Finally, the ***CS** field is a checksum to eliminate garbled messages. The checksum is an 8-bit XOR of the message.

Appendix C: Simulation File Structure and Computational Architecture

The simulation used throughout this research can be found on University of Idaho servers at

\\venus.mrc.uidaho.edu\yelsub\Mechanical\HBL_Simulation\

and operates within the MATLAB programming environment.

The simulation has three main frontend functions: main_GUI.m, main_dataCollect.m, and multi_optimize.m. Each is used to access the same underlying programming for different purposes. The multi_optimize frontend is used to optimize EKF coefficients, allowing a user to specify which coefficients are optimized and other optimization parameters; it calls main_optimize.m, which calls the main simulation function. The main_dataCollect frontend is used to specify a variety of data collection paremeters such as buoy initial location, quantization grid size, or number of Monte Carlo runs to perform. The main_GUI frontend calls a GUI (designed using MATLAB's 'guide' functionality) which can be used to visually evaluate the navigation and error data for the different available mission configurations.

The main simulation function is Navsim_dataCollect.m. It contains the simulation execution loop in which the communication, navigation, noise/error, and state estimation occur. Below is shown the overall information flow structure in the simulation.

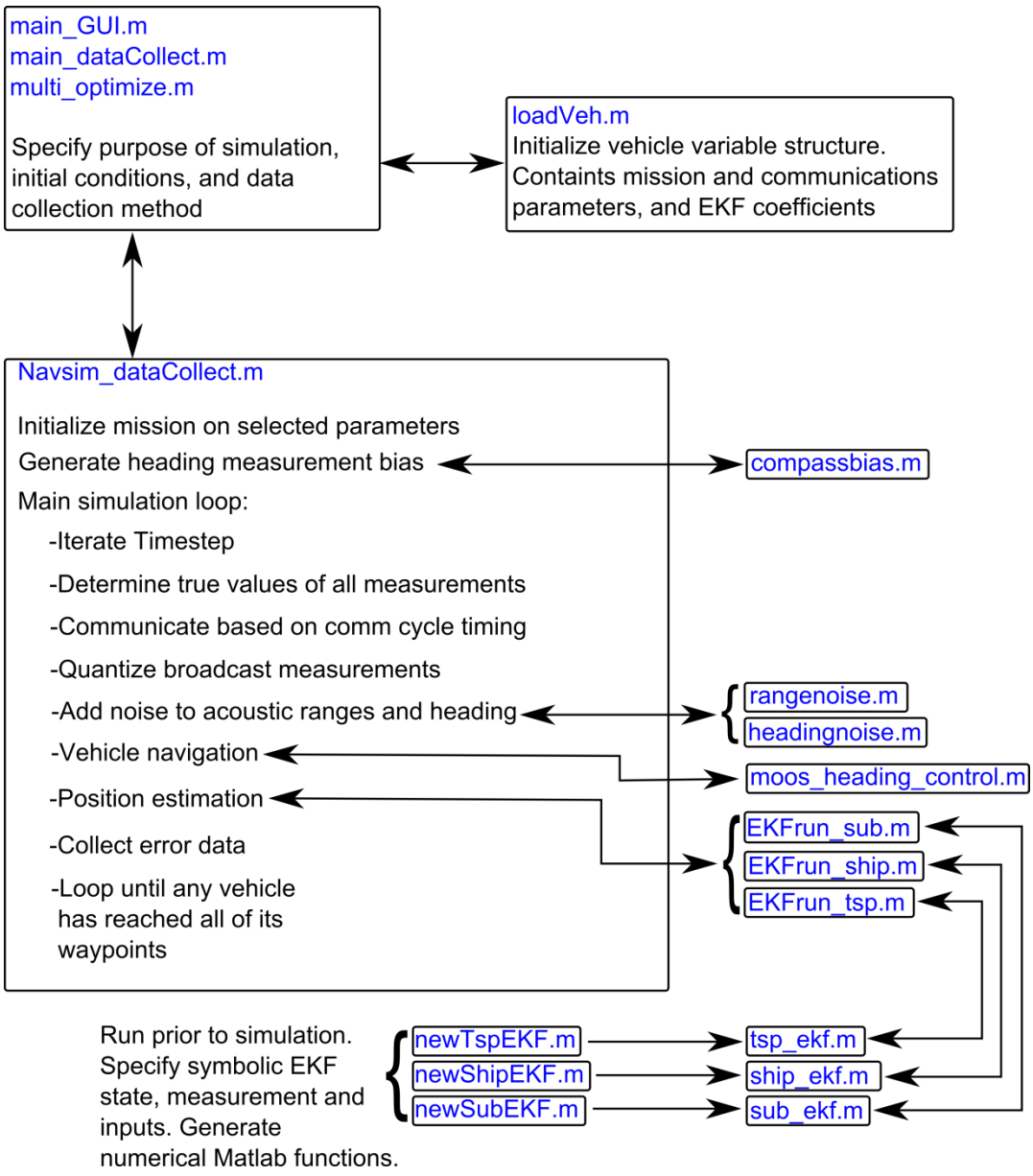
main_GUI.m
main_dataCollect.m
multi_optimize.m
Specify purpose of simulation, initial conditions, and data collection method
loadVeh.m
Initialize vehicle variable structure. Containts mission and communications parameters, and EKF coefficients
Navsim_dataCollect.m
Initialize mission on selected parameters
Generate heading measurement bias
compassbias.m
Main simulation loop:
-Iterate Timestep
-Determine true values of all measurements
-Communicate based on comm cycle timing
-Quantize broadcast measurements
-Add noise to acoustic ranges and heading
rangenoise.m
headingnoise.m
-Vehicle navigation
moos_heading_control.m
-Position estimation
-Collect error data
-Loop until any vehicle has reached all of its waypoints
EKFrun_sub.m
EKFrun_ship.m
EKFrun_tsp.m
Run prior to simulation. Specify symbolic EKF state, measurement and inputs. Generate numerical Matlab functions.
newTspEKF.m
newShipEKF.m
newSubEKF.m
tsp_ekf.m
ship_ekf.m
sub_ekf.m